Dynamic NMR Studies of Chiral 1,1′-Binaphthyl Ligands

Honors Thesis by

G-Yoon Jamie Im

Washington and Lee University

Lexington, Virginia

2002

To my family and friends

and

Marcia

Acknowledgements

First of all I would like to thank my thesis advisor Dr. Marcia France. She has been one of the most amazing minds I've met at Washington and Lee University and an example of a scholar dedicated to chemistry. Her diligent assistance and advice throughout my graduate school search and thesis research make it possible for me to stand at the finish line knowing that I am a more able student of chemistry. She has also been a wonderful mentor and friend during my four year trek through college, and she has always been available when I felt that I needed someone to talk to. She never failed to give me healthy advice, whether it was about people or academics, and I always had the comfort of knowing someone was genuinely concerned about me. Thank you so much for being such an amazing advisor, mentor, and friend to me; I truly don't know how I would have made it through all this without you!

For their help with the NMR, I would like to thank Dr.Ashok Krishnaswami at JEOL, Dr. Erich Uffelman, and Phil Trimmer. Dr.Krishnaswami deserves many thanks for providing us with our spin lock experiment and spending numerous hours with Dr. France, Dr. Uffelman, and Mr.Trimmer on the phone to help us figure out problems we ran into while using the NMR. I would like to thank Dr. Uffelman for acting as the local NMR guru and helping us 24/7 to figure out sources of error messages and save the NMR from potential disaster. I would also like to thank Phil Trimmer for rigging up the N_2 source for the NMR, providing us with ideas on how to fill up that odd Dewar for VT experiments, and giving me a smile every time I trekked down to the basement for numerous hours of experimentation on the NMR.

I would like to thank Dr. Lin Pu at the University of Virginia for allowing us to carry out our NMR studies on his binaphthyl ligand, and his graduate student David Moore for providing us with the binaphthyl ligands. I would also like to thank Jeff Ellena at the Magnetic Resonance Lab of the University of Virginia for helping us with our VT experiments.

Dr. Robert M. Waymouth at Stanford University deserves many thanks as Dr. France learned various aspects of T1ρ experiments at his lab during her sabbatical, allowing for this thesis to exist. I would also like to extend my thanks to Dr. Stephen R. Lynch from the Stanford University Chemistry Department's NMR Facility for passing along his NMR insights to Dr. France, and Dr. Waymouth's graduate student Gregg M. Wilmes for providing us with some crucial advice on calculations.

I would like to also thank the chemistry department at Washington & Lee University for providing me with the background, discipline, and opportunity to work on this thesis. Without each of the chemistry classes I have taken here, I don't think I would have been able to make it through the more challenging phases of thesis work. I would also like to thank the mathematics department at Washington & Lee University for providing me with the tools and confidence to delve into the more complex mathematical formulations of chemistry. Mathematics in journal articles was much more accessible thanks to the years of instruction at Robinson Hall.

Many thanks go to my friends around me, who at all times never failed to tell me that I had what it took for my major. I would also like to thank my fellow chemistry majors who shared my tough but thoroughly rewarding journey through chemistry.

I would like to thank the National Science Foundation's Instrumentation and Laboratory Instruction Program for their funding for the NMR. I would also like to thank Washington and Lee University, the ACS Petroleum Research Fund, the Jeffress Memorial Trust, and Research Corporation for funding Dr. France's work.

Abstract

Chiral monomeric and polymeric binaphthyl ligands have been shown to be highly enantioselective for the asymmetric addition of dialkylzinc and diarylzinc compounds to aldehydes. Previous studies by Pu and coworkers show that differences in efficiencies between monomeric and polymeric ligands hinge on differences in the conformation of the aryl substituents. In order to better understand these chiral binaphthyl ligands, dynamic NMR studies have been undertaken to derive the activation energy and thermodynamic parameters for conformational exchange. Preliminary results give an activation barrier of 6.4 kcal/mol, $\Delta H^{\ddagger}$ value of 6.0 kcal/mol, $\Delta S^{\ddagger}$ value of –21 cal/mol, and $\Delta G^{\ddagger}$ value of 11.7 kcal/mol at 237 K.

Table of Contents

Acknowledgements.....iii

Abstract.....vi

Chapter 1. Dynamic NMR Techniques.....1

Main Concepts in NMR Spectroscopy.....2

Dynamic NMR Techniques.....11

References.....23

Chapter 2. Organozinc Catalysis of Asymmetric Alkyl and Aryl Addition to Aldehydes.....24

Objective of the Thesis.....36

References.....37

Chapter 3. Dynamic NMR Studies of Chiral 1,1′-Binaphthyl Ligands.....38

Introduction.....39

Variable Temperature NMR Studies.....40

$T_{1\rho}$ Experiments.....44

Future Work.....58

Experimental Section.....60

References.....78

Chapter 1

Dynamic NMR Techniques

Nuclear Magnetic Resonance (NMR) techniques are routinely used to deduce the structure of molecules. More recently, NMR has also been used to study chemical exchange rates, rotational frequencies of molecules, and molecular dynamics. Dynamic NMR techniques facilitate the study of the effects of chemical exchange processes and the study of the dynamics of the molecular electronic environment.[1] In this chapter, the main concepts of NMR spectroscopy are introduced and the most commonly used dynamic NMR techniques are surveyed.

Main Concepts in NMR Spectroscopy

A proton has two spin states, and as a charged particle with spin, the proton acts as a little magnet.[2] In the absence of a magnetic field, the two spin states have the same energy value E_a. Thus, the proton spins of a sample are directed in random fashion, much like magnetic chips randomly distributed along a table. When a sample is subjected to the static magnetic field ($\mathbf{B_0}$) of the NMR, the protons of the sample respond by starting to precess around $\mathbf{B_0}$ and orient themselves either parallel or antiparallel to it, depending on their spin (Figure 1).[2]

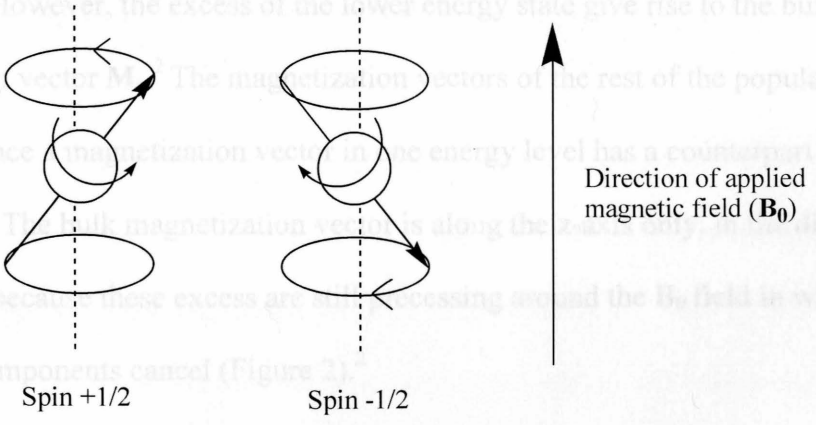

Figure 1. Orientation of protons according to spin.[2]

The frequency of precession is known as the Larmor frequency, denoted as ω. In the external magnetic field, the two spin states (±1/2) of the protons no longer have the same energy. Being antiparallel to the magnetic field requires more energy, and thus -1/2 is the higher energy state.[3] The population of the lower and higher energy states soon equilibrates to match the Boltzmann distribution, the lowest energy state for the system, expressed as:

$$\frac{N_\alpha}{N_\beta} = \exp(-\frac{E_\alpha - E_\beta}{k_B \cdot T}) \quad (1)$$

where N_α and N_β are the number of hydrogen atoms in the lower and higher energy states, respectively, ΔE is the difference in energy between the two states, k_B is Boltzmann's constant, and T is the temperature of the system.[3] Boltzmann's distribution is a dynamic equilibrium model, and members of the higher energy state are free to move down to the lower energy state and vice versa.

Overall, in the presence of a magnetic field there is an excess of protons in the lower energy state as predicted by the Boltzmann distribution, but this excess is very small (1,000,064 in the lower energy state versus 1,000,000 in the higher energy state in a 400 MHz).[2] However, the excess of the lower energy state give rise to the bulk magnetization vector $\mathbf{M_z}$.[2] The magnetization vectors of the rest of the population cancel each other since a magnetization vector in one energy level has a counterpart in the other energy level. The bulk magnetization vector is along the z-axis only, in the direction of the field $\mathbf{B_0}$, because these excess are still precessing around the $\mathbf{B_0}$ field in which the x and y axis components cancel (Figure 2).[2]

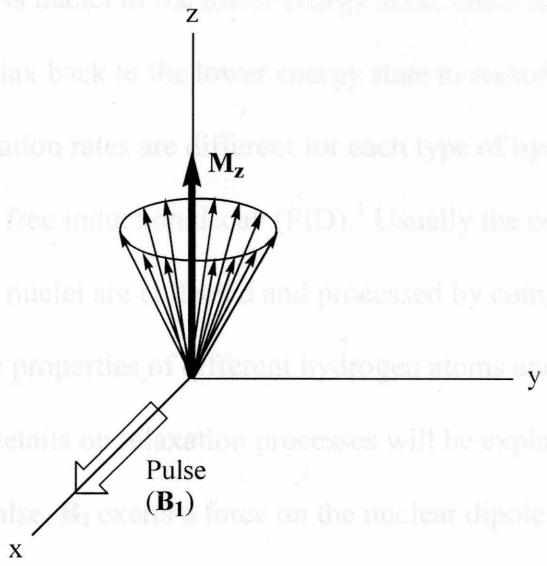

Figure 2. The $\mathbf{M_z}$ bulk magnetization vector and direction of a pulse.[2]

The existence of the bulk magnetization vector permits the study of molecules by NMR. The bulk magnetization vector is manipulated by a pulse, which is a 1 to 10 μs pulse of radiofrequency, where the *rf* frequency matches the Larmor frequency of the nuclei.[4] The field due to the magnetic components of the applied *rf* is generated by alternating voltage across a coil in the probe of the NMR, and the coil is situated in such a way that this alternating magnetic field ($\mathbf{B_1}$) will be perpendicular to $\mathbf{B_0}$.[4] A pulse is thus generated when the perpendicular field $\mathbf{B_1}$ is turned on then turned off after a few microseconds.

In typical NMR experiments, a pulse is applied to flip protons of the lower energy state to the higher energy state, that is, the magnetization vectors of hydrogen nuclei pointing parallel to field $\mathbf{B_0}$ are forced to point antiparallel to it.[2] This inverts the population between the lower and higher energy states, and no net magnetization vector along the z-axis is observed since $\mathbf{M_z}$ arises only due to the individual magnetization

vectors of the excess nuclei of the lower energy state. Once the pulse is stopped, some hydrogen nuclei relax back to the lower energy state to reestablish the Boltzmann distribution. Relaxation rates are different for each type of hydrogen atom, and so each generates a unique free induction decay (FID).[4] Usually the combined FID data for different hydrogen nuclei are collected and processed by computer to give the spectrum used to analyze the properties of different hydrogen atoms and elucidate the structure of a compound. More details on relaxation processes will be explained below.

During a pulse, $\mathbf{B_1}$ exerts a force on the nuclear dipole moment.[4] The 'flipping' of the magnetization vectors of the excess hydrogen nuclei is due to this torque, and the individual hydrogen nucleus that used to precess around $\mathbf{B_0}$ in its own phase now starts to precess around the new field $\mathbf{B_1}$ in phase with all other hydrogen nuclei. This phenomenon of the matching of phases of individual nuclei is known as phase coherence (Figure 3).[2,4]

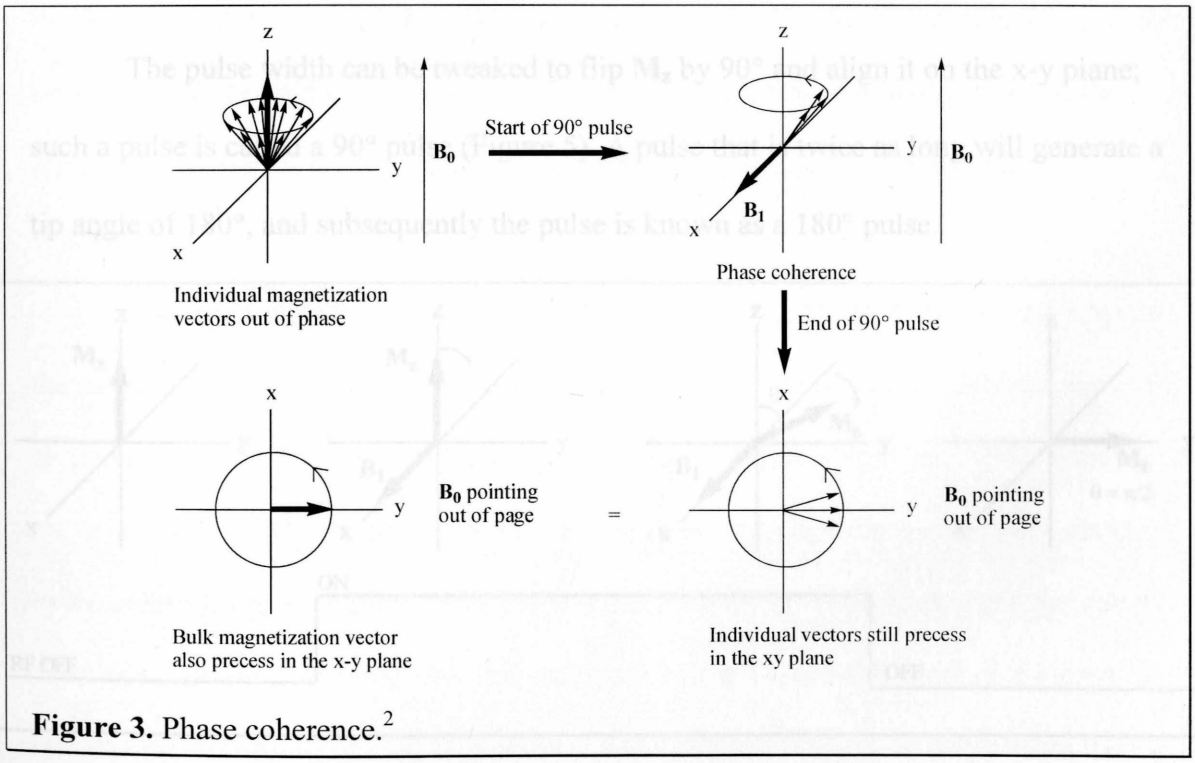

Figure 3. Phase coherence.[2]

Phase coherence leads to a 'bunching' of the magnetization vectors of each nucleus along the y-axis along with the loss of net magnetization along the z-axis. Thus, the bulk magnetization vector $\mathbf{M_z}$ can be 'moved' around the $\mathbf{B_1}$ vector into the xy plane.[4] The duration of the pulse, known as the pulse width, can be adjusted so that $\mathbf{M_z}$ is moved around $\mathbf{B_1}$ at a specific angle, known as the tip angle (Figure 4).[2,4]

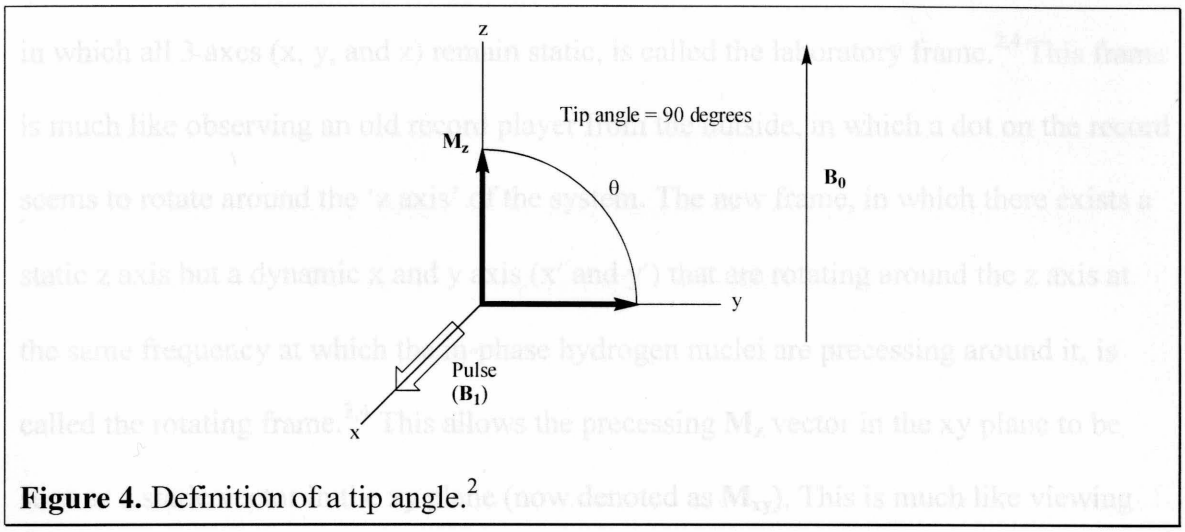

Figure 4. Definition of a tip angle.[2]

The pulse width can be tweaked to flip $\mathbf{M_z}$ by 90° and align it on the x-y plane; such a pulse is called a 90° pulse (Figure 5). A pulse that is twice as long will generate a tip angle of 180°, and subsequently the pulse is known as a 180° pulse.

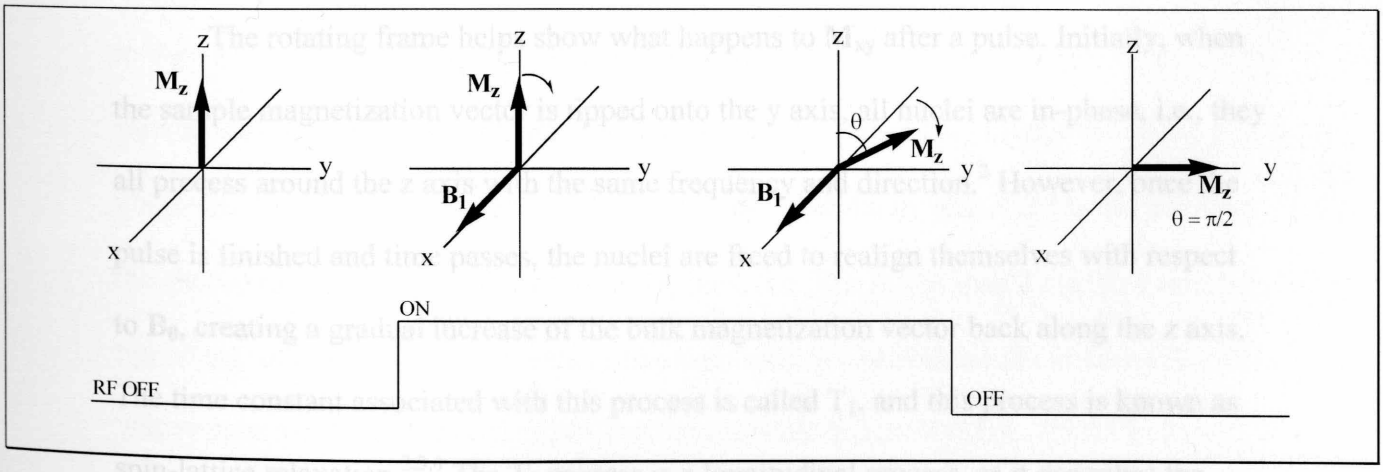

Figure 5. A 90° pulse and the movement of the bulk magnetization vector $\mathbf{M_z}$.[4]

Even after the pulse is applied to $\mathbf{M_z}$, the nuclei that give rise to the bulk magnetization vector are still precessing around $\mathbf{B_0}$. This means that even after $\mathbf{M_z}$ is flipped to the x-y plane, it is precessing around $\mathbf{B_0}$, giving rise to many rotations to consider when studying the motion of the bulk magnetization vector. To further simplify the study of NMR spectroscopy, two frames of view have been defined. The initial frame, in which all 3 axes (x, y, and z) remain static, is called the laboratory frame.[2,4] This frame is much like observing an old record player from the outside, in which a dot on the record seems to rotate around the 'z axis' of the system. The new frame, in which there exists a static z axis but a dynamic x and y axis (x′ and y′) that are rotating around the z axis at the same frequency at which the in-phase hydrogen nuclei are precessing around it, is called the rotating frame.[2,4] This allows the precessing $\mathbf{M_z}$ vector in the xy plane to be seen as a static vector in the xy plane (now denoted as $\mathbf{M_{xy}}$). This is much like viewing the dot on the disc of the old record player while standing on the record; this will give the sense that the dot on the disc is now static. The rotating frame eliminates some of the rotational motions of the magnetization vectors, simplifying calculations and visualization.

The rotating frame helps show what happens to $\mathbf{M_{xy}}$ after a pulse. Initially, when the sample magnetization vector is tipped onto the y axis, all nuclei are in-phase, i.e., they all precess around the z axis with the same frequency and direction.[2] However, once the pulse is finished and time passes, the nuclei are freed to realign themselves with respect to $\mathbf{B_0}$, creating a gradual increase of the bulk magnetization vector back along the z axis. The time constant associated with this process is called T_1, and this process is known as spin-lattice relaxation.[2,3,4] The T_1 process is a longitudinal process, as it describes the

regrowth of $\mathbf{M_z}$ back along the magnetic field vector $\mathbf{B_0}$. Also, without $\mathbf{B_1}$, the nuclei start to randomize in the frequency at which they precess around the z axis, which results in the loss of phase coherence and a decrease of the bulk magnetization vector along the xy plane. The time constant associated with this process is called T_2, and this process is known as spin-spin relaxation.[2,3,4] The T_2 process is not a longitudinal process by definition as it describes the decay of the bulk magnetization vector perpendicular to the magnetic field vector $\mathbf{B_0}$.[3]

These two processes together are used to describe the relaxation phenomena that are crucial for dynamic NMR and all Fourier Transform techniques.[3,4] T_1 relaxation usually contributes to T_2 relaxation, but the time constants associated with these processes are usually not the same.[3] Note that the regrowth of $\mathbf{M_z}$ does not necessarily coincide with the decay of $\mathbf{M_{xy}}$. Such discrepancies are due mainly to dephasing of the individual precessing nuclei (also known as isochromats) caused by the inhomogeneities of the magnetic field $\mathbf{B_0}$ or the natural randomization of nuclei frequencies.[3]

One of the most popular methods of determining T_1 values is the 'inversion-recovery' method, also known as the '180° – τ – 90°' method.[3] As seen in Figure 6, a 180° pulse is delivered to the original bulk magnetization vector, denoted $\mathbf{M_0}$, inverting it to the –z axis. Then, a time interval of τ is allowed to pass to let the hydrogen nuclei relax back along the z-axis, which brings about a partial recovery of $\mathbf{M_0}$. Then, the magnetization vector is hit with a 90° pulse to tip it onto the xy plane. If $\mathbf{M_0}$ did not have the chance to relax back to positive z axis values, (i.e., if τ is less than $T_1/\ln 2$), it will be tipped into the –y axis, which yields an apparent negative peak upon phase-correcting +y values to be positive.[4] If $\mathbf{M_0}$ did relax back to the positive z axis values, it will yield a

positive signal.[3,4] By measuring the magnitude of $\mathbf{M_z}$ at different values of τ, the T_1 value can be obtained with the following equation

$$\mathbf{M_z} = \mathbf{M_0} \cdot (1 - e^{-\tau/T_1}) \quad (2)$$

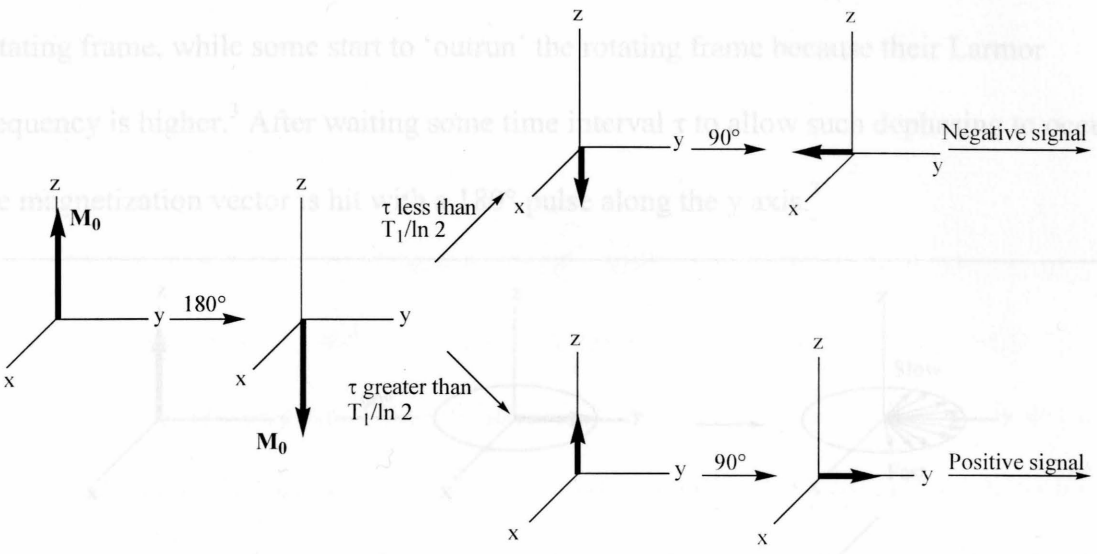

Figure 6. Measurement of T_1.[3]

Accelerated T_1 values can be obtained by control of relaxation pathways available to the hydrogen nuclei.[4] This is frequently done by introduction of paramagnetic compounds into the sample whose unpaired electrons alter T_1 relaxation mechanisms.[4] Accelerated T_1 values are useful in speeding up NMR experiments or increasing the accuracy of quantitative measurements. However, the fact that any paramagnetic substance can alter the T_1 value means that NMR samples need to be degassed; even a minute presence of dissolved oxygen, which is a paramagnetic substance, can significantly decrease the accuracy of T_1 values.[4]

T_2 values are usually determined by the spin-echo experiment.[3,4] First, a 90° pulse is applied to the bulk magnetization vector. The vector, once in the xy plane, starts to

decrease due to effects of natural dephasing along with field inhomogeneity.[3] In the rotating frame, this decrease in the magnitude of $\mathbf{M_{xy}}$ can be easily visualized by observing the isochromats 'fanning out' due to dephasing. As seen in Figure 7, some nuclei start to 'lag' behind because their Larmor frequency is slower than that of the rotating frame, while some start to 'outrun' the rotating frame because their Larmor frequency is higher.[3] After waiting some time interval τ to allow such dephasing to occur, the magnetization vector is hit with a 180° pulse along the y axis.[3]

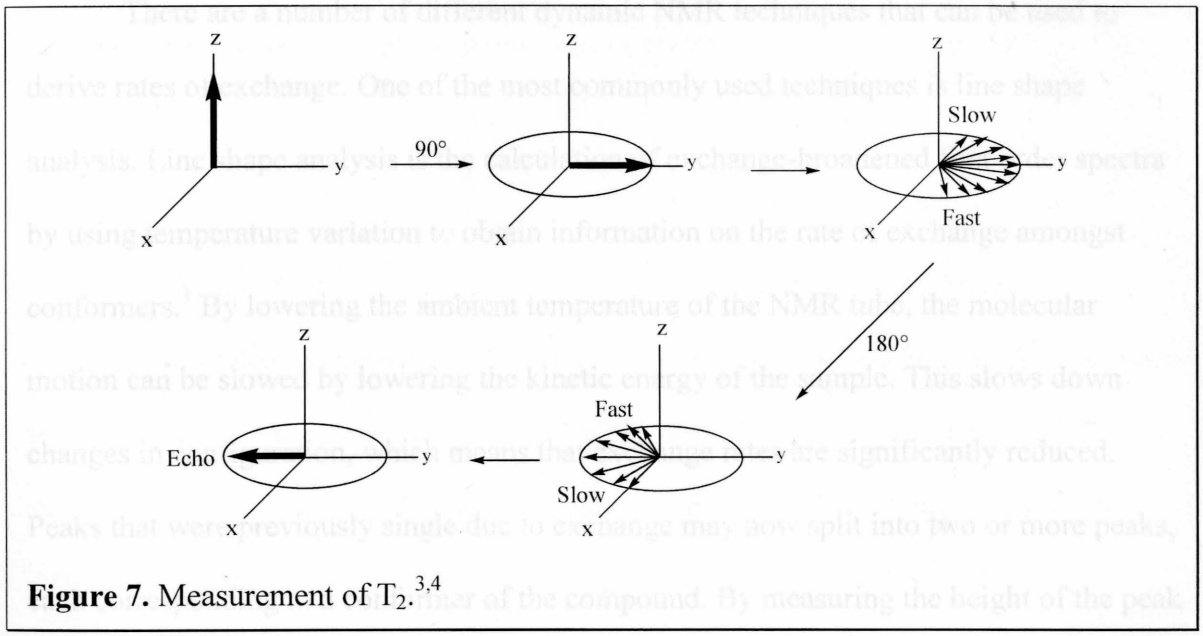

Figure 7. Measurement of T_2.[3,4]

At this point, the magnetization vector of the nuclei lagging behind switch places with those nuclei that are outrunning the rotating frame. However, since the nuclei are still experiencing the same magnetic field $\mathbf{B_0}$ as they had in the beginning of the experiment, the nuclei still move with the same Larmor frequency as they had been before being flipped 180°.[3] A 'refocusing' is observed as isochromats start to move back towards the –y axis, and an echo forms upon completion of refocusing.[3] At the echo, $\mathbf{M_{xy}}$ has grown back to nearly the original length it was at the beginning of the experiment.

The only effect at this point that contributes to any decay of $\mathbf{M_{xy}}$ is due to natural dephasing of nuclei that is completely independent from any effects of the inhomogeneous field.[3] Thus, the amplitude of each subsequent echo shows how $\mathbf{M_{xy}}$ would shrink in a perfectly homogeneous $\mathbf{B_0}$ field, and from this data we can calculate the natural T_2 value.[3]

Dynamic NMR Techniques

There are a number of different dynamic NMR techniques that can be used to derive rates of exchange. One of the most commonly used techniques is line shape analysis. Line shape analysis is the calculation of exchange-broadened first order spectra by using temperature variation to obtain information on the rate of exchange amongst conformers.[1] By lowering the ambient temperature of the NMR tube, the molecular motion can be slowed by lowering the kinetic energy of the sample. This slows down changes in configuration, which means that exchange rates are significantly reduced. Peaks that were previously single due to exchange may now split into two or more peaks, each corresponding to a conformer of the compound. By measuring the height of the peak and linewidths of individual peaks, we can calculate the transverse relaxation time T_2.[1]

The Bloch equations are the fundamental equations of line shape analysis. These equations model the change of the bulk magnetization vector over time along the x, y, and z-axes.[1] They are derived by first defining the change in the bulk magnetization vector after the application of field $\mathbf{B_1}$ in the following manner (equations 3, 4, and 5):

$$\frac{dM_x}{dt} = -\frac{M_x}{T_2} \tag{3}$$

$$\frac{dM_y}{dt} = -\frac{M_y}{T_2} \tag{4}$$

$$\frac{dM_z}{dt} = -\frac{M_z - M_0}{T_1} \tag{5}$$

M_x, M_y, and M_z are the vector components of the bulk magnetization vector being manipulated, and M_0 is the magnitude of the bulk magnetization vector before the application of $\mathbf{B_1}$. The relaxation constants T_1 and T_2 are as defined in the previous sections.

The components of $\frac{dM}{dt}$ along the axes can be calculated via the following determinant constructed from the definitions of a vector product (equation 6):[1]

$$\frac{dM}{dt} = \gamma \begin{vmatrix} M_x & M_y & M_z \\ B_x & B_y & B_z \\ i & j & k \end{vmatrix} \tag{6}$$

where B_x, B_y, and B_z are the vector components of the magnetic fields the bulk magnetization vector experiences (it takes into account both $\mathbf{B_0}$ and $\mathbf{B_1}$), and i, j, and k are the unit vectors of x, y, and z axes. B_z essentially is equivalent to B_0, the magnitude of the static magnetic field along the z axis. $\mathbf{B_1}$ is an alternating magnetic field which can be viewed as the sum of two vectors that are rotating in opposite directions. When the gyromagnetic ratio γ is greater than 0, only the vector with clockwise rotation contributes to the overall motion of $\mathbf{B_1}$, and thus the x and y components of $\mathbf{B_1}$ can be written as:[4]

$$B_{1x} = B_1 \cos 2\pi\nu t \tag{7}$$

$$B_{1y} = -B_1 \sin 2\pi\nu t \tag{8}$$

where ν is the frequency of the *rf* field $\mathbf{B_1}$. B_{1x} and B_{1y} correspond to B_x and B_y of the determinant of equation 6.

The Bloch equations in the laboratory frame are found by developing the determinant of equation 6 and combining it with equations 3, 4, and 5 to give equations 9, 10, and 11:[1]

$$\frac{dM_x}{dt} = \gamma M_y B_0 + \gamma M_z B_1 \sin 2\pi\nu t - \frac{M_x}{T_2} \tag{9}$$

$$\frac{dM_y}{dt} = -\gamma M_x B_0 + \gamma M_z B_1 \cos 2\pi\nu t - \frac{M_y}{T_2} \tag{10}$$

$$\frac{dM_z}{dt} = -\gamma M_x B_1 \sin 2\pi\nu t - \gamma M_y B_1 \cos 2\pi\nu t - \frac{M_z - M_0}{T_1} \tag{11}$$

These Bloch equations can be manipulated to take on a simpler form by interpreting them in the rotating frame.[1] Defining the new axes of the rotating frame with x′ and y′, the components of M in the directions of x′ and y′ are denoted with u and v:[1]

$$M_x = u \cos 2\pi\nu t - v \sin 2\pi\nu t \tag{12}$$

$$M_y = -u \sin 2\pi\nu t - v \cos 2\pi\nu t \tag{13}$$

In conjuction with equation 14, the mathematical definition of the Larmor frequency,

$$\nu_0 = \frac{\gamma B_0}{2\pi} \tag{14}$$

where γ is the gyromagnetic ratio, the Bloch equations in the rotating frame can be derived to be:[1]

$$\frac{du}{dt} = +2\pi v(\nu_0 - \nu) - \frac{u}{T_2} \tag{15}$$

$$\frac{dv}{dt} = -2\pi u(\nu_0 - \nu) - \frac{v}{T_2} - \gamma B_1 M_z \tag{16}$$

$$\frac{dM_z}{dt} = -\frac{M_z - M_0}{T_1} + \gamma B_1 v \tag{17}$$

B_1 denotes the magnitude of the *rf* field $\mathbf{B_1}$, which is now static in the rotating frame. Under slow exchange conditions, the steady state approximation of $\frac{du}{dt} = \frac{dv}{dt} = \frac{dM_z}{dt} = 0$ can be applied.[1] This allows for the values of u, v, and M_z to be calculated:

$$u = \frac{2\pi\gamma B_1 M_0 T_2^2 (v_0 - v)}{1 + 4\pi^2 T_2^2 (v_0 - v)^2 + \gamma^2 B_1^2 T_1 T_2} \tag{18}$$

$$v = \frac{\gamma B_1 M_0 T_2}{1 + 4\pi^2 T_2^2 (v_0 - v)^2 + \gamma^2 B_1^2 T_1 T_2} \tag{19}$$

$$M_z = \frac{[M_0 [1 + 4\pi^2 T_2^2 (v_0 - v)^2]]}{1 + 4\pi^2 T_2^2 (v_0 - v)^2 + \gamma^2 B_1^2 T_1 T_2} \tag{20}$$

The values of u and v are important as they help define the magnetic moment in the xy plane in terms of a complex number G, which is defined to be equal to u + iv.[1] Normal recording conditions are usually carried out below the level of saturation, i.e. $\mathbf{B_1} << 0$, and so the saturation term $\gamma^2 B_1^2 T_1 T_2$ is much less than 1.[1] At such conditions, $\mathbf{M_z} \approx \mathbf{M_0}$ for equation 20, and this yields the following simplified form for G:[1]

$$G = \frac{2\pi C T_2^2 (v_0 - v)}{1 + 4\pi^2 T_2^2 (v_0 - v)^2} - i\frac{C T_2}{1 + 4\pi^2 T_2^2 (v_0 - v)^2} \tag{21}$$

where C is a scaling factor equal to $\gamma B_1 M_0$.

The imaginary part of G, v, gives the absorption bandshape of a group of equivalent nuclei with resonance at ν_0.[1] For a spectrum with equivalent hydrogens appearing at different resonances ν_A and ν_B, expressions for G for site A and site B (G_A and G_B) can be found and the imaginary parts of their sum yields the bandwidths with two Lorentzian absorption bands centered at ν_A and ν_B.[1]

The Bloch equations can then be expanded to accommodate uncoupled two-site exchange models or multi-site exchange models.[6] This allows for the calculation of the height and width of the bandshape of each conformer of the observed peak and natural T_2 values can be derived from the bandshapes.[1,6] The curve with the best rate constants is found by a comparison of the calculated and experimental curves, by visual inspection or by least-squares adaptation.[1]

Once complete separation of a coalesced peak is achieved and a set line shape is established for each temperature interval with equations 18, 19, 20, and 21, the overall rates of exchange can be calculated using the Piette and Anderson derivations.[7] Piette and Anderson's calculation of the approximate expression for the rate constant is based on the population of the conformer A and B (p_A and p_B), T_2 values of each conformer, separation of the conformers in Hz ($\delta\nu$), and the bandwidth W* in the fast exchange region between the two sites of exchange:[7]

$$k_A = 4\pi p_A p_B^2 (\delta\nu)^2 (W^* - \frac{p_A T_{2A} + p_B T_{2B}}{\pi T_{2A} T_{2B}})^{-1} \quad (22)$$

$$k_B = 4\pi p_A^2 p_B (\delta\nu)^2 (W^* - \frac{p_A T_{2A} + p_B T_{2B}}{\pi T_{2A} T_{2B}})^{-1} \quad (23)$$

Line shape analysis over a range of temperatures helps to visualize how each configuration of a molecule is related to one another. In a case where there is a 1:1 distribution of molecules between two different conformations, the two separated peaks at a lower temperature merge towards a midpoint at the same rate (Figure 8).[1]

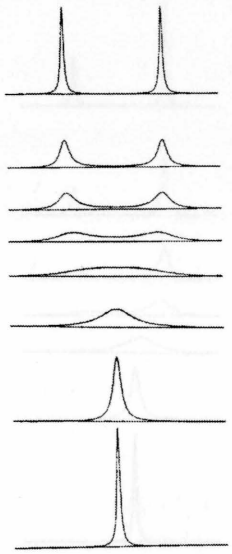

Figure 8. Line shape for a 1:1 population distribution between two states.[8]

However, an unequal population distribution (caused by energetics, sterics, etc.) can greatly alter the manner in which two bands merge; usually, the less intense peak will merge towards the larger peak, and the point at which the two are joined will be skewed towards the peak representing the configuration of the majority of the molecules of a sample. The process of broadening and merging of signals will depend on the relation between the rate constants and the chemical shifts (Figure 9).[1]

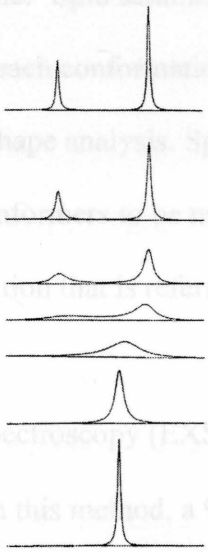

Figure 9. Line shape for an uneven population distribution between two states.[8]

Line shape analysis is a powerful tool for studying complex systems where several simultaneous exchange processes are occurring, since bandshapes are dependent on all rate constants and on the pattern of permutations caused by the exchanges.[1] However, it is limited because it requires that the peaks of interest must be separated completely at some accessible temperature. If this cannot be achieved, it becomes difficult to draw out parameters such as population ratios and the value of the separation between the two peaks that are needed to calculate band shapes and exchange rates.

Spin saturation transfer is another popular dynamic NMR technique used for the calculation of exchange rates. When the system is in the slow exchange region, if complete separation of peaks can be achieved it is possible to selectively irradiate one conformer.[9] This irradiation of one conformer causes saturation to be transferred to the other conformer due to exchange processes.[9] Using the steady state approximation and conditions of chemical equilibrium, we can calculate the exchange rates between two

different conformations of the molecule.[9] Spin saturation transfer also requires complete separation of peaks corresponding to each conformation, which places the same limitation on this experiment as line shape analysis. Spin saturation transfer also requires the exchange rate between the two conformers to be much greater than the relaxation rate of the unirradiated conformer, a condition that is referred to as 'fast exchange on the T_1 time scale'.[9]

Two-dimensional exchange spectroscopy (EXSY) is a third popular method of studying exchange rates by NMR.[10] In this method, a 90° pulse is applied to the bulk magnetization vector along the –x axis, which flips the vector to the –y axis. After a certain length of time t_1 (also known as the labeling time or the evolution time), the vector is hit with another 90° pulse along the –x axis, sending it to the xz plane. A homospoil pulse, a field gradient pulse that removes the x component of the magnetization vector, is applied to derive only the z component of the magnetization vector. After a fixed time t_m (called the mixing time) is allowed for the vector to experience T_1 relaxation, the vector is tipped to the y axis, and the magnetization in the xy plane is measured and stored as a 2-dimensional graph. The cross-peaks in the 2-dimensional spectrum correspond to nuclei that exchange from one site to another.[10] The intensities of the peaks correspond to the exponential of the exchange matrix **R**, and so peak intensities can be used to calculate exchange rate constants.[10] EXSY is especially useful for studies of multi-site exchange systems. However, EXSY, like line shape analysis and spin saturation transfer, requires resolved peaks of each conformer to utilize the exchange matrix **R**.

A lesser-known, but extremely effective, dynamic NMR technique for studying chemical exchange rates is the $T_{1\rho}$ method, where $T_{1\rho}$ is the longitudinal relaxation (T_1) in the rotating frame. The $T_{1\rho}$ method involves 'spin locking' the bulk magnetization vector in the xy plane after a 90° pulse via a continuous wave magnetic field $\mathbf{B_2}$ along the y-axis (Figure 10). As the nuclei start to dephase and the isochromats start to fan after the initial pulse, they start to precess around $\mathbf{B_2}$ even though the original magnetic field $\mathbf{B_0}$ still exists.[3,4] This is because the new magnetic field $\mathbf{B_2}$ is perpendicular to $\mathbf{B_0}$, and so the hydrogen nuclei do not experience the effects of $\mathbf{B_0}$.[4] However, even while spin locked, the bulk magnetization vector still experiences decay in the y axis over time, due to natural T_2 randomization.[3] The time constant associated with the decrease of the bulk magnetization vector within this system is called $T_{1\rho}$, and this phenomenon is known as the spin-lattice relaxation in the rotating frame.[3,4] The reason $T_{1\rho}$ is a type of T_1 relaxation is because the bulk magnetization vector decreases longitudinally along the $\mathbf{B_2}$ axis of force.[3]

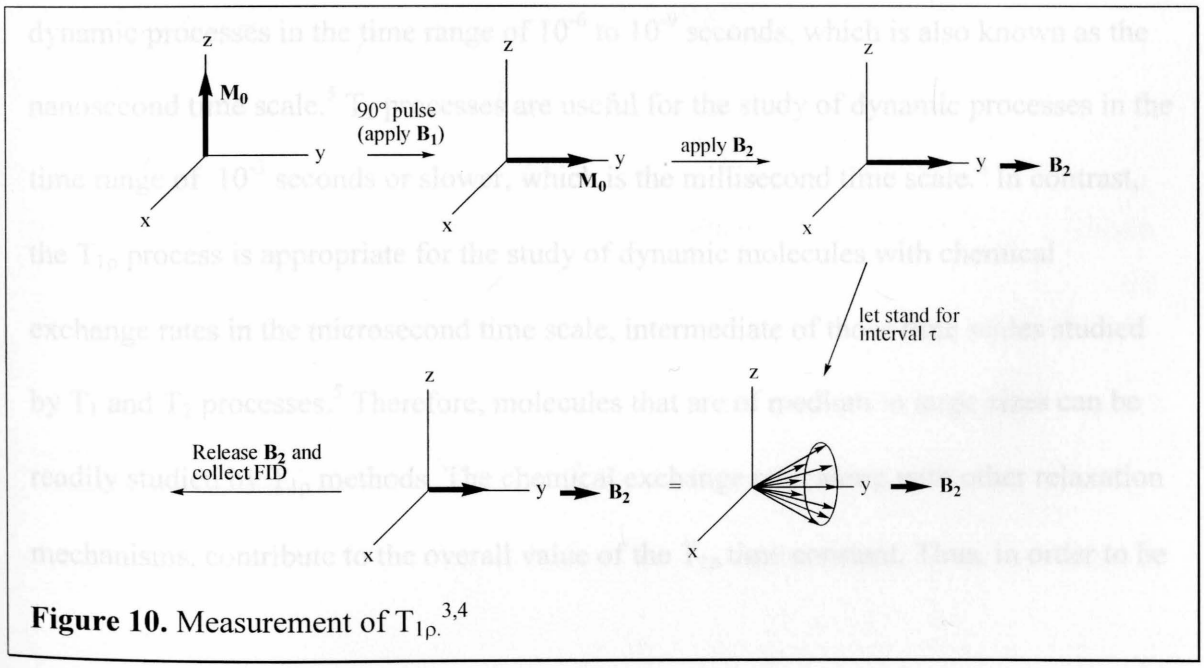

Figure 10. Measurement of $T_{1\rho}$.[3,4]

Experimental methods involve observation of the FID of the bulk magnetization vector in the y-axis of the rotating frame after having spin locked the vector with the new magnetic field $\mathbf{B_2}$ for increasing time intervals of τ (the spin-lock time).[3] This generates, for each iteration, signals with decreasing intensity, since, as observed above, a decay in $\mathbf{M_{xy}}$ is inevitable due to natural T_2 processes. In this manner, the time constant $T_{1\rho}$ (observed) can be calculated by fitting resonance intensities to the expression:[3,4]

$$M_{xy} = M_0 \exp(-\tau/T_{1\rho}) + M' \qquad (24)$$

where M_0 is the original magnitude of the bulk magnetization vector, and M' is a residual signal that is present for long spin-locking times.[11] It is important to note that the above method of determining the $T_{1\rho}$ value is only viable when studying 'on resonance' rotating-frame relaxation.[3] Other methods involving 'off-resonance' rotating-frame relaxation have been developed by Leipert and coworkers.[12]

The values of T_1 and T_2 have been extensively used to measure rate constants, reaction rates, and exchange rates. T_1 processes are especially useful for study of dynamic processes in the time range of 10^{-6} to 10^{-9} seconds, which is also known as the nanosecond time scale.[5] T_2 processes are useful for the study of dynamic processes in the time range of 10^{-3} seconds or slower, which is the millisecond time scale.[5] In contrast, the $T_{1\rho}$ process is appropriate for the study of dynamic molecules with chemical exchange rates in the microsecond time scale, intermediate of those time scales studied by T_1 and T_2 processes.[5] Therefore, molecules that are of medium to large sizes can be readily studied by $T_{1\rho}$ methods. The chemical exchange rate, along with other relaxation mechanisms, contribute to the overall value of the $T_{1\rho}$ time constant. Thus, in order to be

able to calculate the exchange rates of the hydrogens of interest, it is crucial to separate the contributions due to other relaxation mechanisms.[5]

In 1970, Deverell and coworkers determined that the $T_{1\rho(ex)}$ (the contribution to $T_{1\rho}$ due to exchange mechanisms) can be calculated as follows:[13]

$$\frac{1}{T_{1\rho(ex)}} = \frac{1}{T_{1\rho(obs)}} - \frac{1}{T_1} \tag{25}$$

However, Deverell and coworkers assumed that the spin-rotation interactions that contribute to the $T_{1\rho}$ value were short, which leads to the assumption that the corresponding rotational correlation time τ_c was short.[13] Thus, Deverell assumed that the value of $\omega_0\tau_c$, where ω_0 is the Larmor frequency of the hydrogen nuclei, was much less than 1. That is, Deverell assumed that the value of $\omega_0\tau_c$ was in the 'extreme narrowing condition.'[5] Wang, in a paper published in 1992, noted that the extreme narrowing condition is a situation suitable for rapidly tumbling small molecules, and that $T_{1\rho(ex)}$ values for molecules of medium to large sizes need to be considered in a different light.[5] Wang proposed that $T_{1\rho(ex)}$ can be calculated from the following

$$\frac{1}{T_{1\rho(ex)}} = \frac{1}{T_{1\rho(obs)}} - \frac{1}{T_{1\rho(dd)}} \tag{26}$$

where $T_{1\rho(dd)}$ is the dipolar rotating-frame relaxation rate.[5] Evaluation of $T_{1\rho(dd)}^{-1}$ involves the calculation of a ratio between $T_{1\rho(dd)}^{-1}$ and T_1^{-1} using the rotational correlation time τ_c, since the ratio is essentially made up of only spectral density functions and τ_c.[5] τ_c values can be found by using the ratio of T_1 and T_2 values or the ratio between selective and nonselective T_1 values.[5,14,15] Using measured T_1 values and the ratio calculated with τ_c,

$T_{1\rho(dd)}^{-1}$ can be calculated, and thus the value for $T_{1\rho(ex)}^{-1}$ can be evaluated using equation 23.[5]

The $T_{1\rho}$ method is useful because no peak separation is required for the peak of interest. Calculations can be done on the coalesced peak, which is useful for those compounds whose motions are difficult to 'freeze out'.

A survey of dynamic NMR spectroscopic methods show that not many are suited for the studies of conformational exchange for those molecules whose motions are difficult to freeze out. The $T_{1\rho}$ method is of great interest since not only it is able to draw out exchange rates, but also the chemical shift separation between peaks belonging to different conformations and the rate constant k of exchange. From these values, thermodynamic parameters ($\Delta G^{\ddagger}$, $\Delta H^{\ddagger}$, $\Delta S^{\ddagger}$, and activation energy E_A) can be derived for the exchange between conformers. Further details on abstracting such rate data will be discussed in chapter 3.

References

(1) Sandström, J. *Dynamic NMR Spectroscopy*; Academic Press: New York, 1982.

(2) Pavia, D. L.; Lampman, G. M.; Kriz, G. S. *Introduction to Spectroscopy: A Guide for Students of Organic Chemistry*, 2nd ed.; Saunders College Publishing: Philadelphia, Pennsylvania, 1995.

(3) Traficante, D. D. In *Encyclopedia of NMR*; Grant, D. M., Harris, R. K., Eds.; Wiley & Sons: New York, 1996; Vol. 6, pp 3988 – 4003.

(4) Derome, A. E. In *Modern NMR Techniques for Chemistry Research*; Baldwin J. E., Magnus, P. D., Eds.; Tetrahedron Organic Chemistry Series; Pergamon Press: Elmsford, NY, 1993; Vol. 6.

(5) Wang, Y. S. *Concepts Magn. Reson.* **1992**, *4*, 327-337.

(6) McConnell, H. M. *J. Chem. Phys.* **1958**, *20*, 430.

(7) Piette, L. H.; Anderson, W. A. *J. Chem. Phys.* **1959**, *30*, 899-908.

(8) Figures from Sandström, J. *Dynamic NMR Spectroscopy*; Academic Press: New York, 1982; pp 15-16.

(9) Neuhaus, D.; Williamson, M. P. *The Nuclear Overhauser Effect in Structural and Conformational Analysis*, 2nd ed.; Methods in Stereochemical Analysis; Wiley-VCH: New York, 2000.

(10) Perrin C. L.; Dwyer, T. J. *Chem. Rev.* **1990**, *90*, 935-967.

(11) Ravikumar, M.; Shukla, R.; Bothner-By, A. A. *J. Chem. Phys.* **1991**, *95*, 3092-3098.

(12) Leipert, T. K.; Noggle, J. H.; Freeman, W. J.; Dalrymple D. L. *J. Magn. Reson.*, **1975**, *19*, 208-221.

(13) Deverell, C.; Morgan, R. E.; Strange, J. H. *Mol. Phys.* **1970**, *18*, 553-559.

(14) Davis, D.G. *J. Am. Chem. Soc.* **1987**, *109*, 3471-3472.

(15) Mirau, P.A.; Bovey, F.A. *J. Am. Chem. Soc.* **1986**, *108*, 5130-5134.

Chapter 2

Organozinc Catalysis of Asymmetric Alkyl and Aryl Addition to Aldehydes

The creation of asymmetric compounds is of great interest in many fields such as pharmaceuticals and biotechnology, since nature's mechanism of recognizing molecules is not only based on composition, but also on the three dimensional orientation of a compound.[1] Many biologically active compounds contain multiple chiral centers, thus a major drive in organic synthesis is finding methods of creating such chiral centers with high enantioselectivity.

The synthesis of chiral secondary alcohols is a subfield that has been studied extensively because secondary alcohols are major components of many natural products, biologically active compounds, and materials such as liquid crystals.[2] They are also important as synthetic intermediates for the generation of halide, amine, ester, and ether functionalities.[2] Diarylcarbinols, a specific type of chiral secondary alcohol, are useful as synthetic intermediates for biologically active compounds.[3]

Two methods for the enantioselective synthesis of chiral secondary alcohols are the enantioselective alkylation of aldehydes and the enantioselective reduction of ketones, as shown in Figure 1.[2] Enantioselective alkylation of aldehydes is of particular interest because it not only creates a chiral center, but also a carbon-carbon bond, which is important in building the backbone of an organic compound.[1,2]

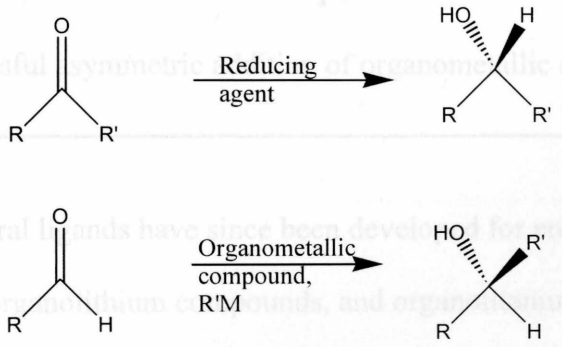

Figure 1. Two methods of synthesis of chiral secondary alcohols.

Enantioselective alkylation of aldehydes can be carried out by organometallic compounds, a class of molecules that have been extensively studied since the first known organozinc compound was created by Frankland in 1849.[1,2,4] However, from Grignard reagents to organolithium compounds, early attempts at enantioselective alkylation of aldehydes with organometallic compounds were met with mediocre enantioselectivities.[2]

In the 1980s, significant steps were made towards achieving over 90% ee with the enantioselective alkylation of aldehydes. The first successful attempt was by Mukaiyama and coworkers, adding alkyllithium and dialkylmagnesium compounds to aldehydes in the presence of a lithium salt of the chiral diamino alkoxide **1** derived from (S)-proline to yield products with up to 95% ee, as shown in Scheme 1.[5]

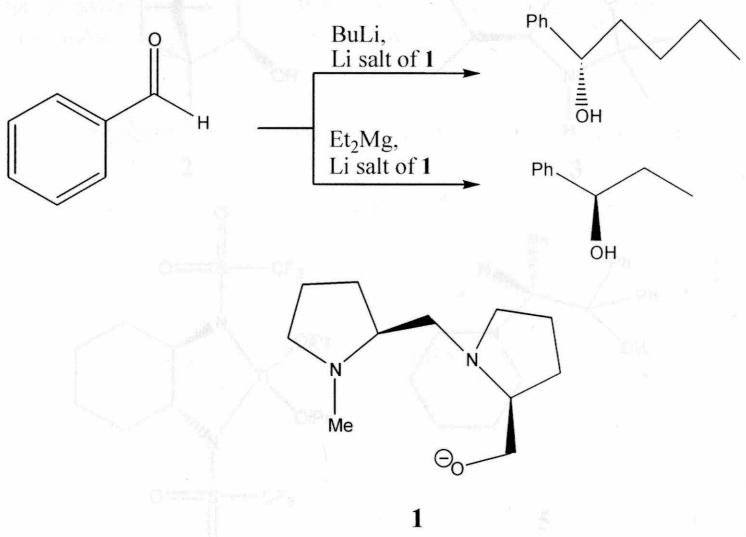

1

Scheme 1. First successful asymmetric addition of organometallic compounds to aldehydes.

Many other chiral ligands have since been developed for enantioselective addition of Grignard reagents, organolithium compounds, and organotitanium compounds to aldehydes, but many are limited by the need for stoichiometric or even an excess amount

of the chiral ligand. This difficulty arises mainly because the achiral pathway is competitive with the chiral pathway catalyzed by the ligands.[2]

In 1986, Noyori and coworkers succeeded in developing the first highly enantioselective amino alcohol catalyst for the asymmetric reaction of dialkylzinc complexes with aldehydes.[6] Dialkylzinc complexes are useful since the uncatalyzed addition reaction of dialkylzinc compounds is much slower than the catalyzed addition reaction. Since 1986, many other chiral ligands have been developed, several of which are shown in Figure 2.[6,7,8,9,10] However, many such ligands are effective for catalysis of the addition reaction only to certain types of aldehydes.[7]

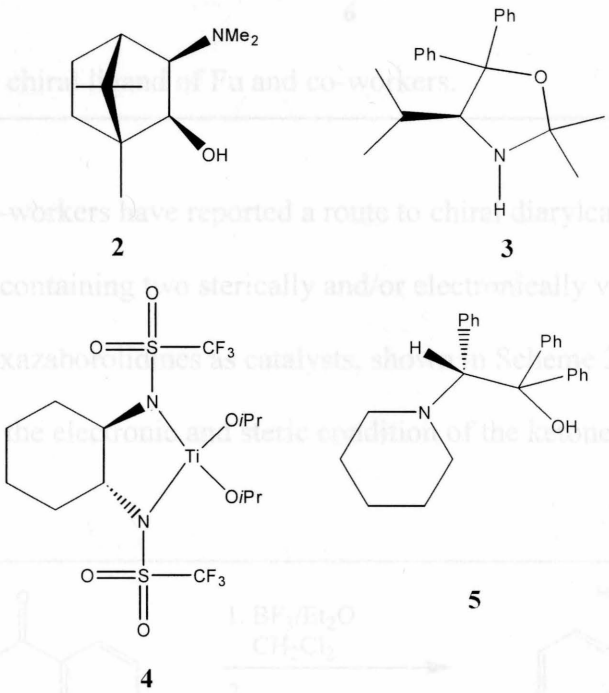

Figure 2. Ligands for dialkylzinc addition to aldehydes.

In a similar vein, in 1997 Fu and coworkers described the first enantioselective catalytic addition of diphenylzinc to aldehydes based on a planar chiral ligand (**6**),

presented in Figure 3.[7,11] However, the addition of diphenylzinc to *p*-chlorobenzaldehyde yielded a moderate 57% ee, since unlike the diethylzinc addition to aldehydes, the uncatalyzed diphenylzinc addition to aldehydes is competitive with the catalyzed reaction.[12] Thus, some of the substrate was being channeled into the nonselective pathway, lowering enantioselectivity.[12]

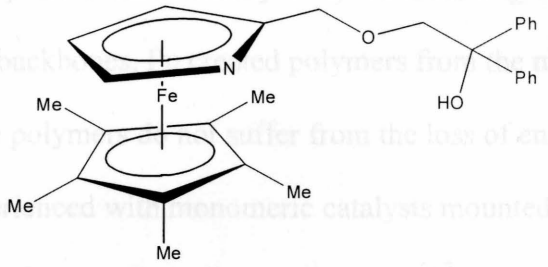

6

Figure 3. The planar chiral ligand of Fu and co-workers.

Corey and co-workers have reported a route to chiral diarylcarbinols by the reduction of ketones containing two sterically and/or electronically very different aryl groups using chiral oxazaborolidines as catalysts, shown in Scheme 2.[13] However, due to severe limitations on the electronic and steric condition of the ketone, this reaction is still very limited.

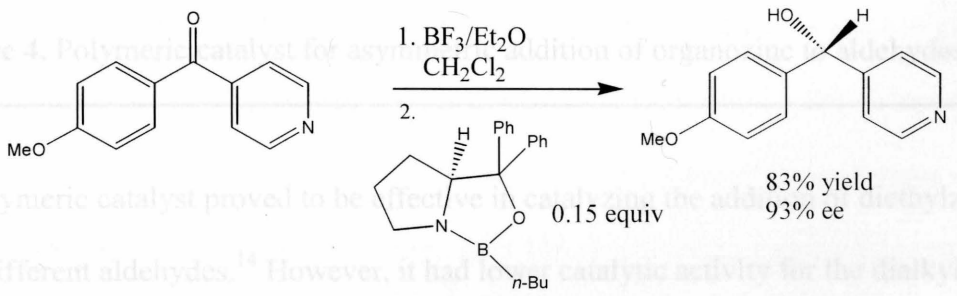

Scheme 2. Reduction of ketones with sterically or electronically different aryl groups.

In 1998, Pu, Hwang, and Hu reported a highly enantioselective (over 95% ee) chiral polymeric binaphthyl catalyst for the reaction of diethylzinc with aromatic aldehydes, shown in Figure 4.[14] Polymeric catalysts have the advantage of being easier to recover and reuse than monomeric catalysts, which is of great interest in industry since the preparation of chiral catalysts is an expensive endeavor.[7] Unlike previous attempts at developing catalytic polymers, which mainly involved mounting catalytic monomer units onto irregular polymer backbones, Pu created polymers from the monomeric catalysts themselves. Thus, these polymers do not suffer from the loss of enantioselective catalytic activity frequently experienced with monomeric catalysts mounted on polymers, because the microenvironments of the catalytic sites are preserved.[7]

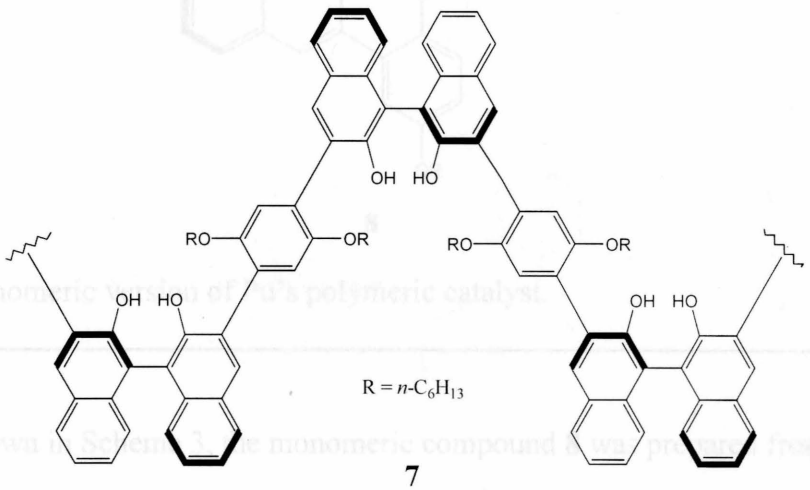

7

Figure 4. Polymeric catalyst for asymmetric addition of organozinc to aldehydes.

The polymeric catalyst proved to be effective in catalyzing the addition of diethylzinc to many different aldehydes.[14] However, it had lower catalytic activity for the dialkylzinc addition to *o*-substituted benzaldehydes and aliphatic aldehydes.[14] Initial variation of the size of the R groups on the alkoxyphenylene linkers did not increase catalytic activity for

these reactions. Thus, a monomeric version of the biphenyl polymer **7** was prepared in order to gain an understanding of the function of the polymer and to improve its catalytic properties.[14,15] The monomer **8** (Figure 5) was shown to be an extremely effective catalyst for the enantioselective alkylation of aldehydes yielding % ee values of 95 or higher.[7,14] **8** was also shown to be the most general ligand for a large variety of aldehydes.[7,14]

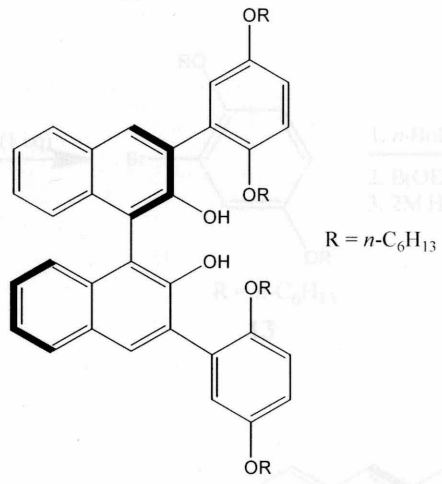

8

Figure 5. Monomeric version of Pu's polymeric catalyst.

As shown in Scheme 3, the monomeric compound **8** was prepared from optically pure (*R*)-1,1′-bi-2-naphthol (**9**). First, the hydroxyls were protected as methoxymethyl groups by treatment with sodium hydride followed by chloromethyl methyl ether to give **10**. Iodide was added to the 3,3′-positions by reaction with *n*-butyllithium followed by iodine to yield **11**. The side-arm aryl compound **14** was generated by a series of reactions of 1,4-dihydroquinone. A bromine atom was removed from **12** with 1 equivalent of *n*-butyllithium to give compound **13**. Compound **13** was converted into **14**, a monoboronic

acid, by reaction with another equivalent of *n*-butyllithium followed by triethylborate. Suzuki coupling between compounds **11** and **14** followed by hydrolysis generated **8**. [7,15]

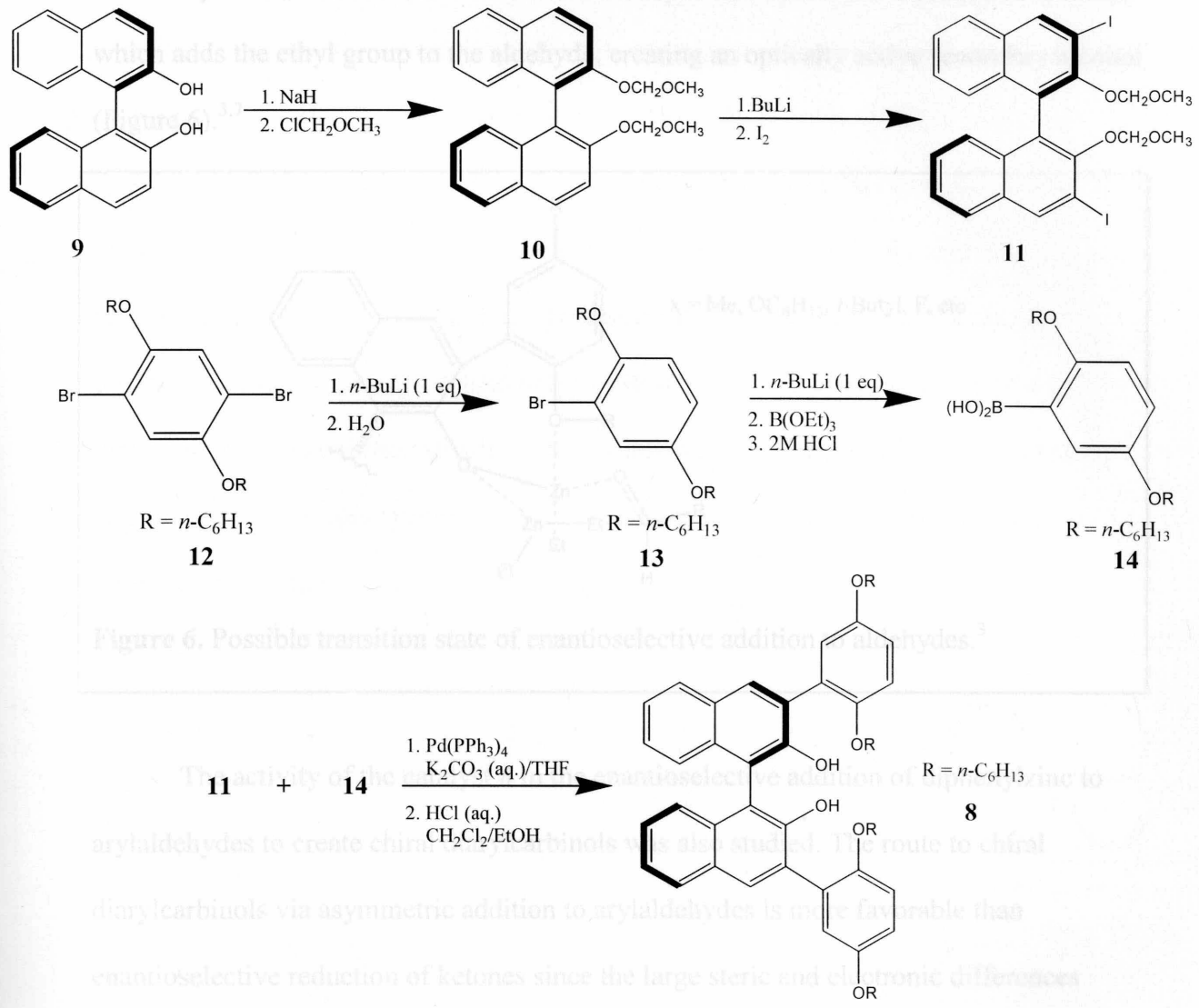

Scheme 3. Synthesis of the monomeric ligand **8**.

Compound **8** with diethylzinc was found to catalyze reactions of para-, ortho-, or meta-substituted aromatic aldehydes with high enantioselectivities. It was also found to effectively catalyze diethylzinc addition with linear or branched aliphatic aldehydes and

aryl or alkyl substituted α,β-unsaturated aldehydes.[7] It is necessary to have two equivalents of diethylzinc for each equivalent of ligand, and this is thought to create a zinc complex that attacks the *re* face of the aldehyde and carries out a concerted reaction, which adds the ethyl group to the aldehyde, creating an optically active secondary alcohol (Figure 6).[3,7]

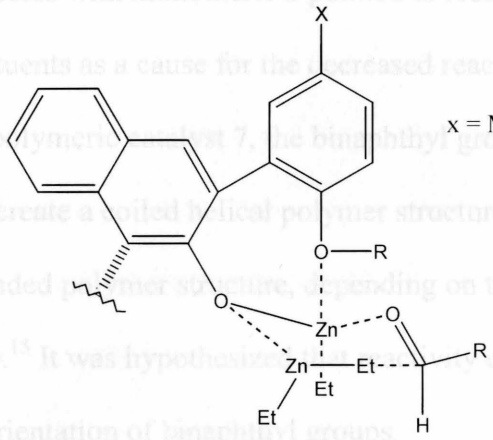

Figure 6. Possible transition state of enantioselective addition to aldehydes.[3]

The activity of the catalyst **8** in the enantioselective addition of diphenylzinc to arylaldehydes to create chiral diarylcarbinols was also studied. The route to chiral diarylcarbinols via asymmetric addition to arylaldehydes is more favorable than enantioselective reduction of ketones since the large steric and electronic differences between the aryl group and the hydrogen on the aldehyde is more suitable for asymmetric induction than the differences between the two aryl groups on the ketone.[12] Catalyst **8** proved to be effective in this reaction, opening a route to enantioselective synthesis of diarylcarbinols. The diarylcarbinol reaction was further optimized by using diethylzinc to pre-treat **8**, lowering concentrations of substrates, and using methanol as an additive for asymmetric addition to α,β-unsaturated aldehydes.[12]

Derivatives of **8** with electron withdrawing groups on the 3-aryl substituent of the binaphthyl unit have been prepared and shown to activate the catalyst further.[3] The electron withdrawing group pulls electron density away from the oxygen atom on the substituent arm, which in turn allows the zinc atom with which it is complexed to become a stronger Lewis acid, further activating the aldehyde.[3]

The studies with monomeric **8** pointed to restrictions in the rotational motion of the aryl substituents as a cause for the decreased reactivity of the polymeric catalyst. In the restricted polymeric catalyst **7**, the binaphthyl groups can be in either a cisoid orientation to create a coiled helical polymer structure or in a transoid orientation to create an extended polymer structure, depending on the orientation of the 3,3'-aryl side arm (Figure 7).[15] It was hypothesized that reactivity of the polymer depended upon its 3-dimensional orientation of binaphthyl groups.

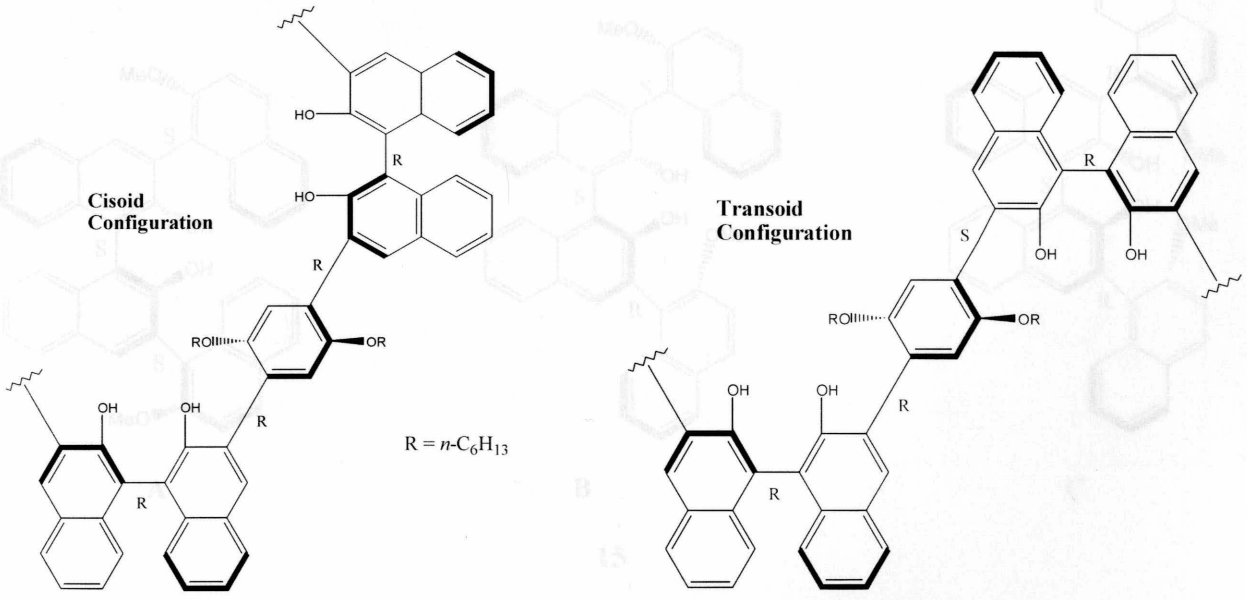

Figure 7. Cisoid and transoid configuration of binaphthyl polymer.[15]

In order to investigate this hypothesis, a derivative of monomer **8** was prepared that had bulky binaphthyl substituents on the binaphthyl ring, which restricted the rotational freedom of the monomeric catalyst, imitating the environments of the polymeric catalyst. Studies on the monomeric (*S*)-1,1'-binaphthyl ligand **15** show that there are 3 different conformations of the ligand that coordinate to the zinc center in different manners, as seen in Figure 8.[15] X-ray structure studies of conformer **A** and computational studies of conformer **B** and **C** indicate that **A** has the least degree of oxygen coordination – 2 versus 3 or 4 in the other two conformers – which allows the zinc center to have the highest Lewis acidity, leading to the highest catalytic activity.[15] Thus, a (*S,S*)-3,3'-aryl conformation for the (*S*)-1,1'-binaphthyl ligand is shown to have the highest catalytic activity.

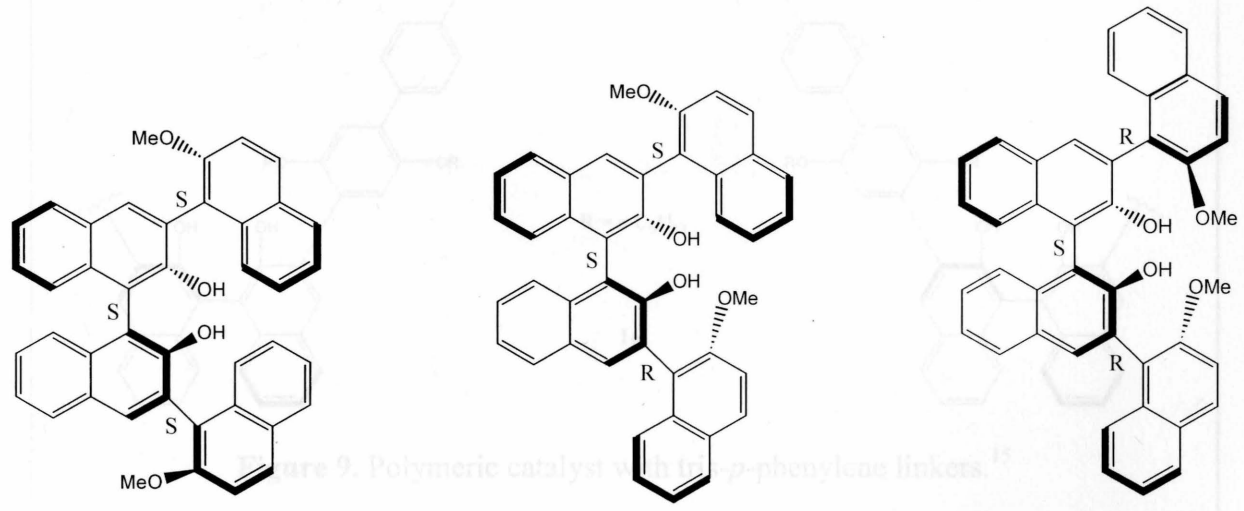

A **B** **C**

15

Figure 8. Three conformations of the monomeric ligand **15**.[15]

Upon preparation of polymeric catalyst **16**, with the monomeric units connected with rigid tris-*p*-phenylene linkers (Figure 9), the polymer displayed almost the same high, general catalytic activity as the monomer.[15] Compared to polymer **7**, the orientation of the 3,3'-aryl subsituents no longer dictates the relative orientation of the biphenyl units, and this lead to the increase in catalytic activity.[15] Thus, the steric environment as well as the electric environment is crucial for reactivity of the polymeric catalysts for enantioselective addition to aldehydes.

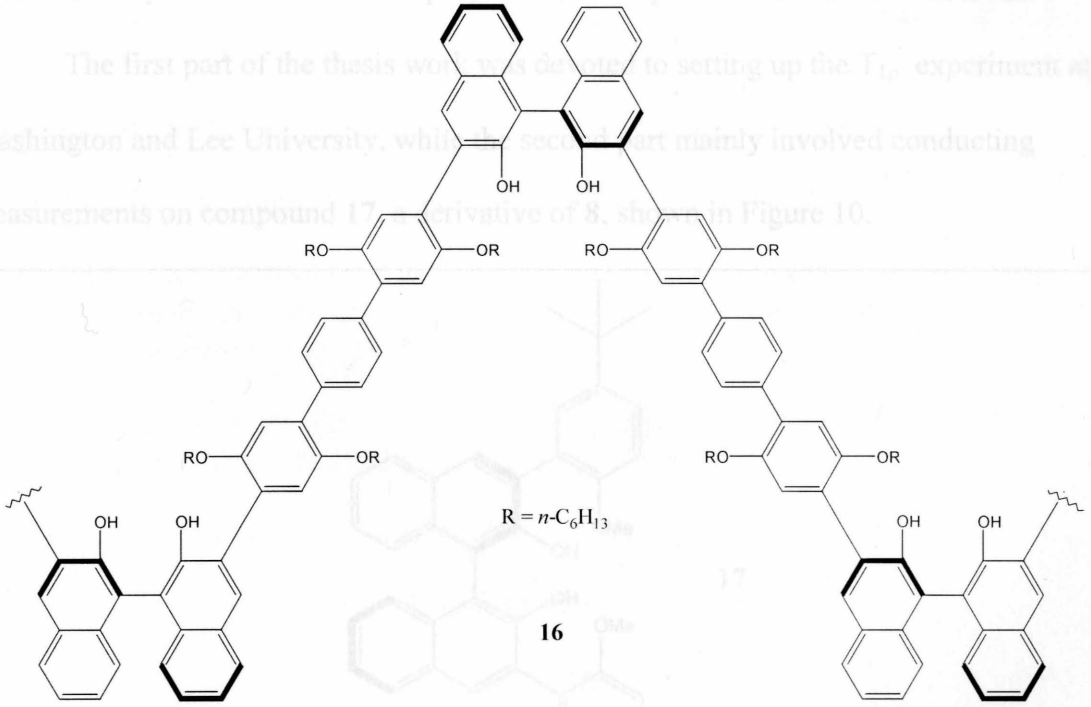

16

Figure 9. Polymeric catalyst with tris-*p*-phenylene linkers.[15]

Objective of the Thesis

Due to the significance of binaphthyl and aryl substituent conformation on the reactivity of the catalytic polymers, further studies on the physical parameters of the exchange between different conformations of the monomer is of great interest. The goal of this thesis is to measure the rate of exchange and the activation barrier between conformations of binaphthyl ligands similar to ligand **8** using dynamic NMR techniques. The $T_{1\rho}$ method was chosen for the main method of study since the anticipated rotation rates of the aryl substituents would prove to be too rapid for conventional methods.

The first part of the thesis work was devoted to setting up the $T_{1\rho}$ experiment at Washington and Lee University, while the second part mainly involved conducting measurements on compound **17**, a derivative of **8**, shown in Figure 10.

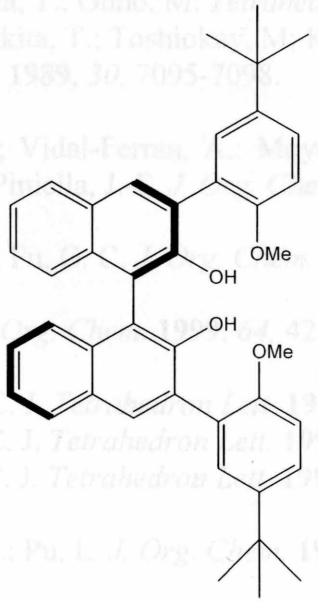

17

Figure 10. Binaphthyl monomer studied.

References

(1) Noyori, R.; Kitamura, M. *Angew. Chem. Int. Ed. Engl.* **1991**, *30*, 49-69.

(2) Soai, K.; Niwa S. *Chem. Rev.* **1992**, *92*, 833-856.

(3) Huang, W.-S.; Pu, L. *Tetrahedron Lett.* **2000**, *41*, 145-149.

(4) Frankland, E. *Ann. Chem. Pharm.* **1849**, *71*, 171-213.

(5) (a) Soai, K.; Mukaiyama, T. *Chem. Lett.* **1978**, 491.
(b) Sato, T.; Soai, K.; Suzuki, K.; Mukaiyama, T. *Chem. Lett.* **1978**, 601.
(c) Mukaiyama, T.; Soai, K.; Sato, T.; Shimizu, H.; Suzuki, K. *J. Am. Chem. Soc.* **1979**, *101*, 1455-1460.

(6) Kitamura, M.; Suga, S.; Kawai, K.; Noyori, R. *J. Am. Chem. Soc.* **1986**, *108*, 6071-6072.

(7) Huang, W.-S.; Hu, Q.-S.; Pu, L. *J. Org. Chem.* **1999**, *64*, 7940-7956.

(8) Prasad, K. R. K.; Joshi, N. N. *J. Org. Chem.* **1997**, *62*, 3770-3771.

(9) (a) Yoshioka, J.; Kawakita, T.; Ohno, M. *Tetrahedron Lett.* **1989**, *30*, 1657-1660.
(b) Takahashi, H.; Kawakita, T.; Toshiokay, M; Kobayashi, S.; Ohno, M. *Tetrahedron Lett.* **1989**, *30*, 7095-7098.

(10) Solà, L.; Reddy, K. S.; Vidal-Ferran, A.; Moyano, A.; Pericàs, M. A.; Riera, A.; Alvarez-Larena, A.; Piniella, J.-F. *J. Org. Chem.* **1998**, *63*, 7078-7082.

(11) Dosa, P. I.; Ruble, J. C.; Fu, G. C. *J. Org. Chem.* **1997**, *62*, 444-445.

(12) Huang, W.-S.; Pu, L. *J. Org. Chem.* **1999**, *64,* 4222-4223.

(13) (a) Corey, E. J.; Helal, C. J. *Tetrahedron Lett.* **1995**, *36*, 9153.
(b) Corey, E. J.; Helal, C. J. *Tetrahedron Lett.* **1996**, *37*, 4837 – 4840.
(c) Corey, E. J.; Helal, C. J. *Tetrahedron Lett.* **1996**, *37*, 5675 – 5678.

(14) Huang, W.-S.; Hu, Q.-S.; Pu, L. *J. Org. Chem.* **1998**, *63*, 1364-1365.

(15) Simonson, D.; Kingsbury, K.; Xu, M.-H.; Hu, Q.-S.; Sabat, M.; Pu, L. Submitted to *Tetrahedron.*

Chapter 3

Dynamic NMR Studies of Chiral 1,1′-Binaphthyl Ligands

Introduction

Asymmetric addition of alkyl and aryl groups to aldehydes to create chiral secondary alcohols is of particular interest in synthetic organic chemistry as it generates compounds with chiral centers and extends the carbon backbone of a molecule.[1,2] The most effective asymmetric addition of alkyl and aryl groups to aldehydes is catalyzed by organozinc compounds coupled with chiral ligands. Recently, Pu, Hwang, and Hu succeeded in creating polymeric binaphthyl catalysts that are extremely effective at synthesizing asymmetric chiral secondary alcohols.[3]

Due to the significance of binaphthyl and aryl substituent conformations on the reactivity of the catalytic polymers described in Chapter 2, further studies on the physical parameters of the exchange between different conformations of the monomeric species are of great interest. Ligand **1** was chosen as a model compound to derive the rate of exchange and the activation barrier between conformations. Ultimately, other derivatives of the monomeric species with different alkyl and alkoxyl substituents on the aryl ring will also be studied.

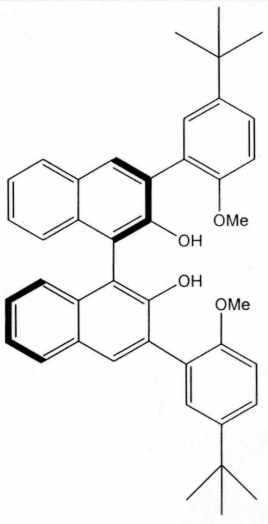

1

Figure 1. Binaphthyl monomer studied.

Variable Temperature NMR Studies

The ^{1}H-NMR spectrum of ligand **1** at room temperature showed a single peak each for the methoxy and *t*-butyl protons, indicative of a rapid rotation about the naphthyl-aryl bond. Changes in line shape of the ^{1}H-NMR spectrum with respect to temperature were studied to see if peak separation could be achieved for the peaks of interest. Initial studies at room temperature in $CDCl_3$ at 400 MHz did not show separation of the methoxy or *tert*-butyl hydrogen peaks at –49.5 °C, about 10° above the freezing point of $CDCl_3$ (–63 °C). However, since peak broadening was observed, the solvent was switched to methylene chloride-d_2, which has a freezing point of –95 °C, to access a lower temperature range. At –70.0 °C, the methoxy peak started to split into two peaks, and by –80.3 °C, four overlapping peaks appeared (Figure 2). Similar separation patterns were also observable in the *t*-butyl peak. Complete resolution was not possible at the temperature range available to the solvent.

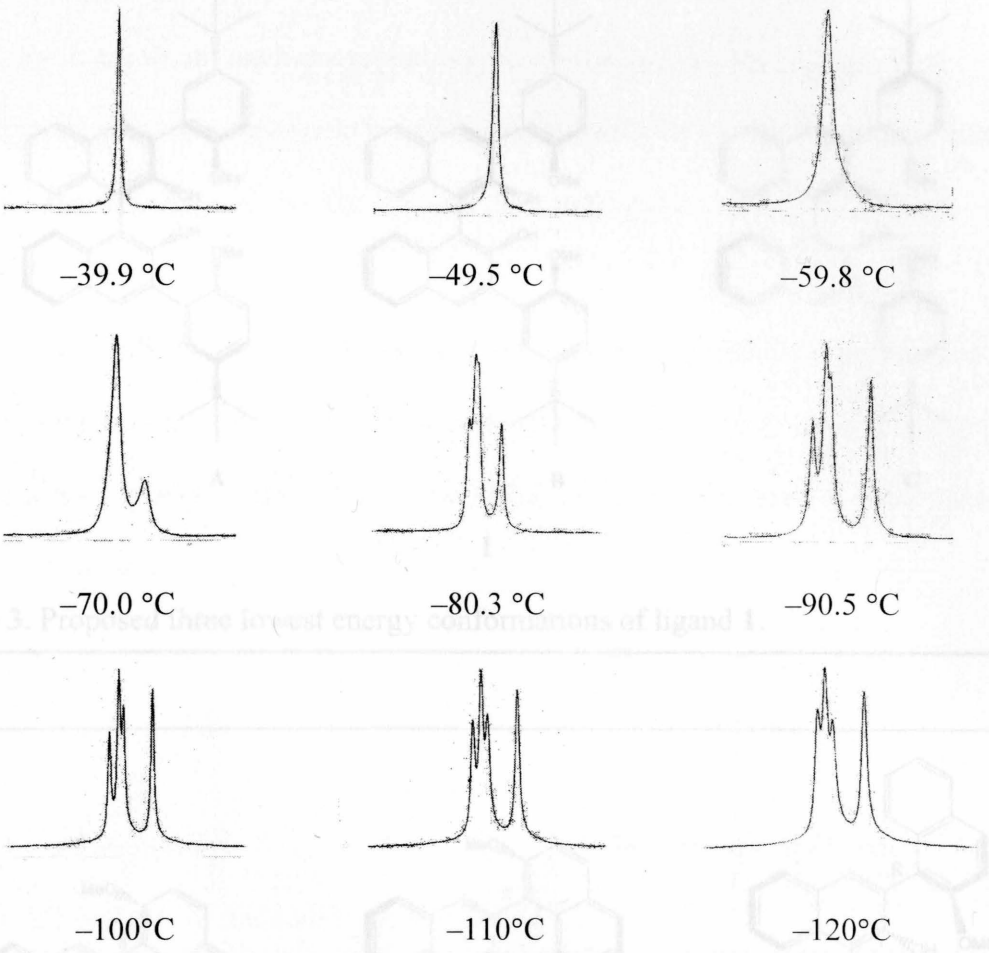

Figure 2. ^{1}H-NMR spectra of the methoxy peak from –39.9 °C to –120 °C.[a,b]

[a]In CD_2Cl_2 from –39.9 °C to –80.3 °C and in DCFM-*d* from –90.5 °C to –120 °C. [b]Corrected temperatures are shown up to –90.5 °C (400 MHz JEOL NMR) and set temperatures are shown from –100 °C to –120 °C (500 MHz Varian NMR, not calibrated).

Separation of the methoxy peak indicated that lowering the temperature slowed the rotation rate of the aryl substituent. It is believed that the four peaks correlate to the favored conformations (i.e., the lowest energy conformations) of ligand **1**, analogous to those observed for the sterically bulky binaphthyl substituents in ligand **2** (Figures 3 and 4).[4]

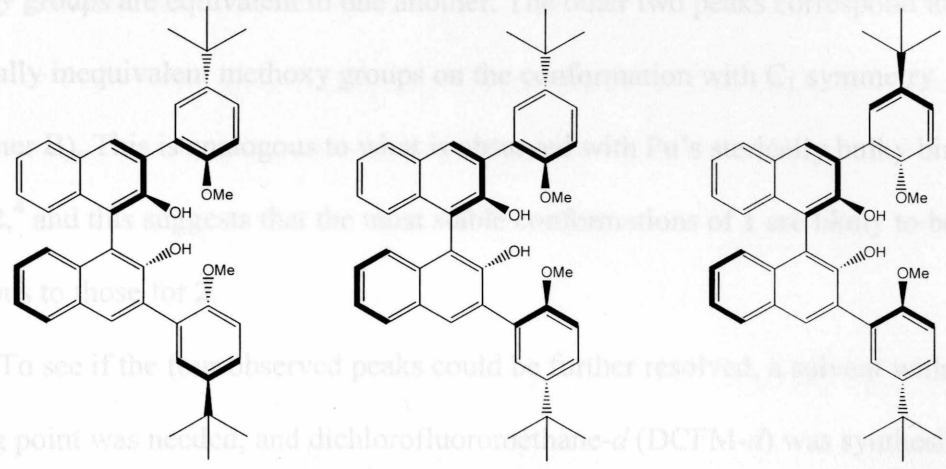

1

Figure 3. Proposed three lowest energy conformations of ligand **1**.

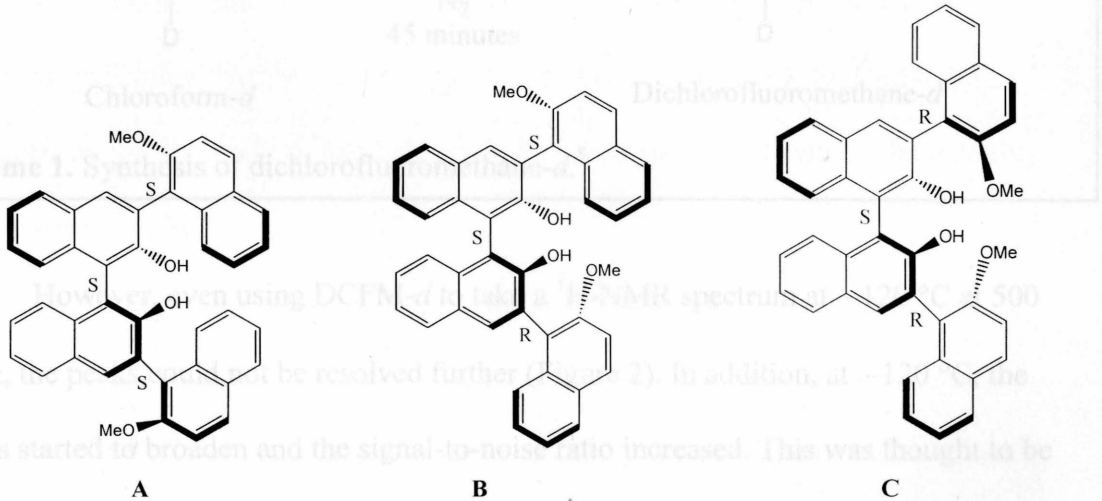

2

Figure 4. Three lowest energy conformations observed for ligand **2**.[4]

The three lowest energy conformations for ligand **1** (Figure 3) would be expected to give rise to a total of four peaks. Two peaks correspond to the methoxy group on each of the conformations with C_2 symmetry (confomers A and C). In these conformations, the

methoxy groups are equivalent to one another. The other two peaks correspond to the chemically inequivalent methoxy groups on the conformation with C_1 symmetry (confomer B). This is analogous to what is observed with Pu's sterically bulky binaphthyl ligand **2**,[4] and this suggests that the most stable conformations of **1** are likely to be analogous to those for **2**.

To see if the four observed peaks could be further resolved, a solvent with a lower freezing point was needed, and dichlorofluoromethane-*d* (DCFM-*d*) was synthesized by reacting antimony trichloride, antimony pentafluoride, and chloroform-*d* under static nitrogen (Scheme 1).[5]

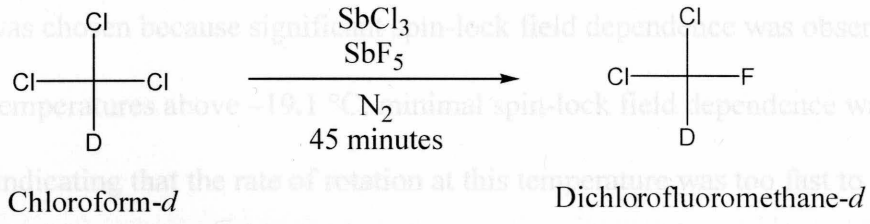

Chloroform-*d* Dichlorofluoromethane-*d*

Scheme 1. Synthesis of dichlorofluoromethane-*d*.[5]

However, even using DCFM-*d* to take a ^{1}H-NMR spectrum at –120 °C at 500 MHz, the peaks could not be resolved further (Figure 2). In addition, at –120 °C, the peaks started to broaden and the signal-to-noise ratio increased. This was thought to be caused either by the fact that the experimental conditions were approaching the freezing point of the solvent or by the lower solubility of the binaphthyl compound at this temperature.

Since complete peak separation was not possible, line shape analysis could not be used for determination of rate constants and other physical parameters. This also ruled out the use of other dynamic NMR techniques such as EXSY and spin saturation transfer,

as these methods also require complete separation of the peak of interest. The $T_{1\rho}$ method was thus an appropriate method to use as measurements can be done on the coalesced peak at temperatures at or above –59.8 °C.

$T_{1\rho}$ Experiments

On-resonance $T_{1\rho}$ values were measured at different spin-locking field strengths ranging from 109 Hz to 3857 Hz over a range of temperatures from –19.1°C to –59.8°C. Temperature calibration experiments were carried out using literature procedures with a methanol calibration NMR tube insert and CD_2Cl_2.[6] The temperature range of –19.1 °C to –59.8 °C was chosen because significant spin-lock field dependence was observed in this range. At temperatures above –19.1 °C, minimal spin-lock field dependence was observed, indicating that the rate of rotation at this temperature was too fast to be measured by the $T_{1\rho}$ method. Just below –59.8 °C was the point at which the methoxy peak started to split.

As discussed in Chapter 1, $T_{1\rho}$ values can be obtained by monitoring the relaxation of the bulk magnetization vector over time at each spin-lock field. Thus, individual $T_{1\rho}$ values ($T_{1\rho(obs)}$) were found by manually measuring the methoxy peak height (M_{xy}) at each spin lock time τ, and plotting the natural log of the peak heights versus the spin lock time τ. The equation

$$\ln M_{xy} = \ln M_0 - \frac{\tau}{T_{1\rho}} \quad (1)$$

where M_{xy} is the height of the methoxy peak at spin-locking time τ and M_0 is the original magnitude of the bulk magnetization vector in the absence of a spin-locking field, was

used for the linear regression analysis.[7] A source of error for the calculation of $T_{1\rho}$ values was that in some cases, the computer was unable to phase all of the individual peaks in all the arrayed spectra, affecting the height. This happens because the computer attempts to find phasing parameters for the full spectrum and then apply it across the entire series of spectra. As the experiment is done on-resonance, peaks off the center of the spectral window may be unphasable. This difficulty can be corrected by individual phasing of the peak of interest in each spectrum, and further studies should be devoted to such error corrections.

The T_1 values were measured, and the unweighted value was used to calculate $T_{1\rho(ex)}$ according to equation:[8]

$$\frac{1}{T_{1\rho(ex)}} = \frac{1}{T_{1\rho(obs)}} - \frac{1}{T_1} \qquad (2)$$

The $T_{1\rho}$ data were used to determine rate constants under an equally populated 2-state assumption, although this is not a correct description of the system. This simplified approach has been taken in other complex systems, such as the study of conformations of complex cyclic octapeptides by Wang and Kopple.[9] Although variable temperature NMR studies revealed that there are 3 unequal populations for the conformation of ligand **1**, Wang and Kopple's example demonstrates that an estimate for the exchange rates and activation barriers can be found with the 2-state assumption and can be used for comparison studies.[9] A series of comparisons between binaphthyl ligands with different alkyl and alkoxy groups on the aryl substituent is planned for the future, and thus the 2-state assumption was an acceptable option. The exchange rate between conformers and

the chemical shift separation were therefore derived using the Deverell approximation for two equally populated states:[8]

$$\frac{1}{T_{1\rho(ex)}} = \frac{1}{T_{1\rho(obs)}} - \frac{1}{T_1} = \frac{(\Delta\nu)^2}{4} \cdot \frac{\tau_{exch}}{1+\omega^2\tau_{exch}^2} \tag{3}$$

where ω is the power of the spin-locking field in radians per second, $\Delta\nu$ is the chemical shift difference between the exchanging protons in the absence of chemical exchange (in rad sec^{-1}), and τ_{exch} is the effective lifetime of the exchanging protons. Plotting $T_{1\rho(ex)}$ versus the square of the field strength in radians yields a straight line with the slope = $4\tau_{exch}/(\Delta\nu)^2$ and an intercept = $4/(\Delta\nu)^2\tau_{exch}$. From these equations, individual expressions for τ_{exch}, $\Delta\nu$, and the rate constant k are derived:[8]

$$\tau_{exch} = \left(\frac{\text{slope}}{\text{intercept}}\right)^{1/2} \tag{4}$$

$$k = 1/(2\tau_{exch}) \tag{5}$$

$$\Delta\nu = \left(\frac{4\tau_{exch}}{\text{slope}}\right)^{1/2} \tag{6}$$

The spin-locking field strength is varied by changing the attenuator setting (dB value) in the NMR acquisition parameters. To obtain field strengths at each attenuator setting, the 90° pulse widths (PW90) needed to be determined. PW90 experiments were carried out at room temperature. Initial PW90 experiments showed that PW90 was 9.8 μs at 0 dB. However, when the PW90 experiment at 0 dB was repeated after a couple of months, the PW90 was found to be 12.2 μs, which was much higher than previously measured. A third PW90 experiment at 0 dB two months later gave a pulse width of 8.9 μs and subsequently lower pulse widths at dB 17, 20, and 25 than those values predicted

earlier from 9.8 μs as PW90. Due to time constraints and difficulty with the instrument, it was not possible to finish compiling the PW90 for the other dB values.

PW90 values from 30 dB to 48 dB were thus extrapolated by first generating expected PW90 values using 8.9 μs as the starting value and using the fact that PW90 doubles for every 6 dB increase. The 8.9 μs was used as the starting value as it was obtained when most of the $T_{1\rho}$ experiments were being run. The measured values for dB 17, 20, and 25 were added to the list of approximated PW90 values (since the above method generated PW90 values for dB 6, 12, 18, etc) and exponential regression analysis was carried out on these points to generate an idealized curve of predicted and measured values. Then, PW90 values for dB 30, 33, 36, 39, 42, 45, and 48 were calculated from the regression analysis equation. Data for measured and projected values are presented in Table 1, and the regression analysis graph is presented in Graph 1.

Table 1. Approximated and measured PW90 values.

dB	PW90 (microseconds) - Measured and projected values
0	8.9
6	17.8
12	35.6
17	68.2
18	71.2
20	97.5
24	142.4
25	174.3
30	284.8
36	569.6
42	1139.2
48	2278.4
54	4556.8
60	9113.6

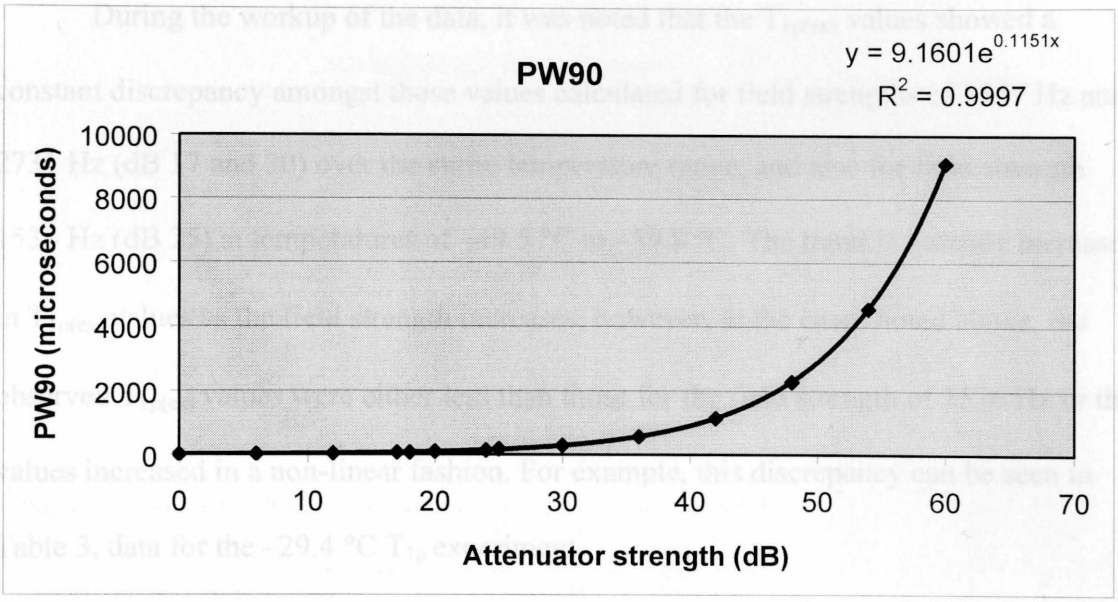

Graph 1. Regression analysis for derivation of projected PW90 values.

With the calculated PW90 values from regression analysis, the field strengths (ω) were calculated using the equation:

$$\omega = \frac{1}{4 \cdot \mathrm{PW90}} \tag{7}$$

where the PW90 value is in seconds. The field strength was multiplied by 2π to convert it into units of radians/second and then squared to obtain values of ω^2.[10] The results are summarized in Table 2.

Table 2. Calculation of field strength at each dB.

dB	PW90 (μs) – Calculated from regression	ω (Hz)	ω (rad s^{-1})
0	8.9	27292	171482.4
17	68.2	3857	24234.6
20	97.5	2731	17158.3
25	174.3	1536	9650.2
30	289.4	864	5427.5
33	408.8	612	3842.7
36	577.4	433	2720.7
39	815.5	307	1926.3
42	1151.8	217	1363.8
45	1626.8	154	965.6
48	2297.7	109	683.6

During the workup of the data, it was noted that the $T_{1\rho(ex)}$ values showed a constant discrepancy amongst those values calculated for field strengths of 3857 Hz and 2731 Hz (dB 17 and 20) over the entire temperature range, and also for field strength 1536 Hz (dB 25) at temperatures of –49.5 °C to –59.8 °C. The trend is a steady increase in $T_{1\rho(ex)}$ values as the field strength increases; however, in the cases noted above, the observed $T_{1\rho(ex)}$ values were either less than those for the field strength of 1536 Hz or the values increased in a non-linear fashion. For example, this discrepancy can be seen in Table 3, data for the –29.4 °C $T_{1\rho}$ experiment.

Table 3. Data for the –29.4 °C $T_{1\rho}$ experiment.

ω (Hz)	$T_{1\rho(obs)}$ (sec)	$T_{1\rho(ex)}$ (sec)
3857	0.4608	2.968614
2731	0.4677	3.280395
1536	0.4476	2.49466
864	0.409	1.634771
612	0.3591	1.051018
433	0.3257	0.808389
307	0.3004	0.668622
217	0.2848	0.595964
154	0.274	0.550554
109	0.2736	0.548941

Because this inconsistency seemed to be due to a systematic problem, $T_{1\rho(ex)}$ values for field strengths 3857 Hz and 2731 Hz were dropped for each temperature and the $T_{1\rho(ex)}$ values for field strength 1536 Hz were dropped for temperatures from –49.5 °C and –59.8 °C before determining the rate parameters and $\Delta\nu$ values via equations 3, 4, and 5. Following these omissions, plots of $T_{1\rho(ex)}$ versus ω^2 at each temperature gave a straight line. An example of the data for the field lock strengths from 109 Hz to 1536 Hz for –19.1 °C, –29.4 °C, and –39.9 °C, and for the field lock strengths from 109 Hz to 864 Hz for –49.5 °C and –59.8 °C can be found in Graph 2 through Graph 6.

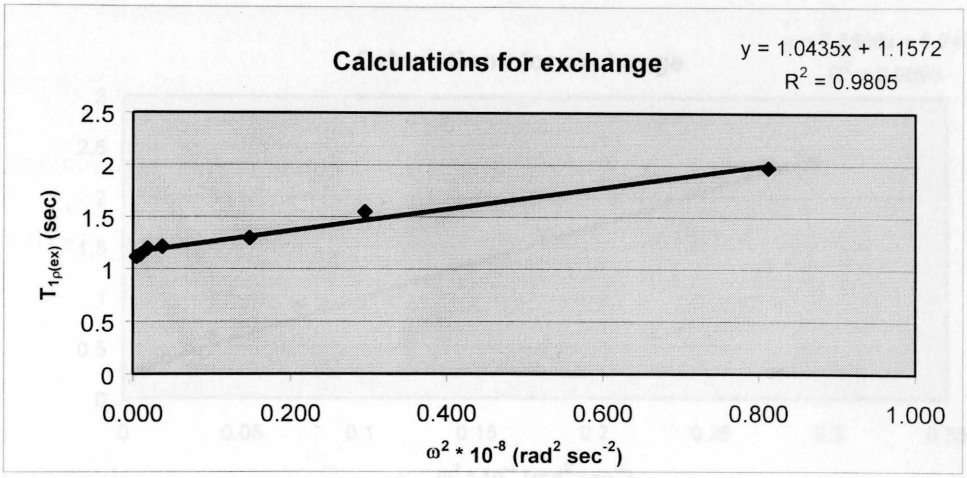

Graph 2. Linear regression analysis for –19.1 °C experiment.

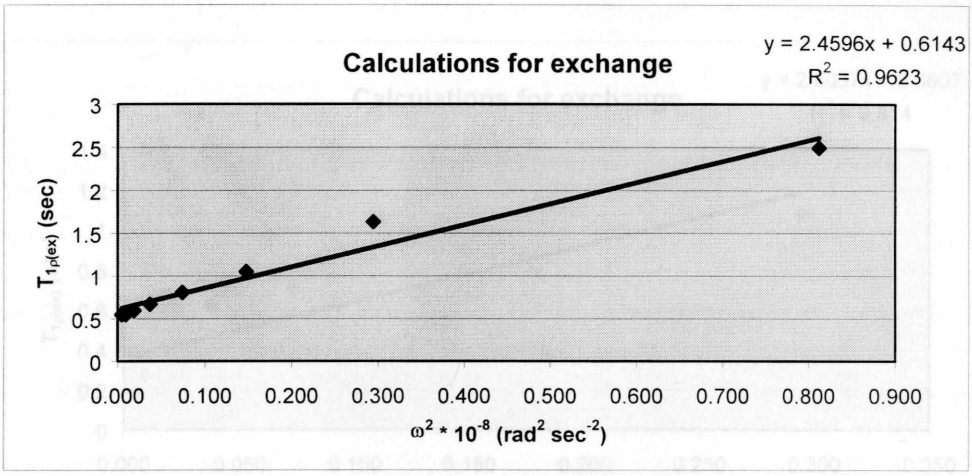

Graph 3. Linear regression analysis for –29.4 °C experiment.

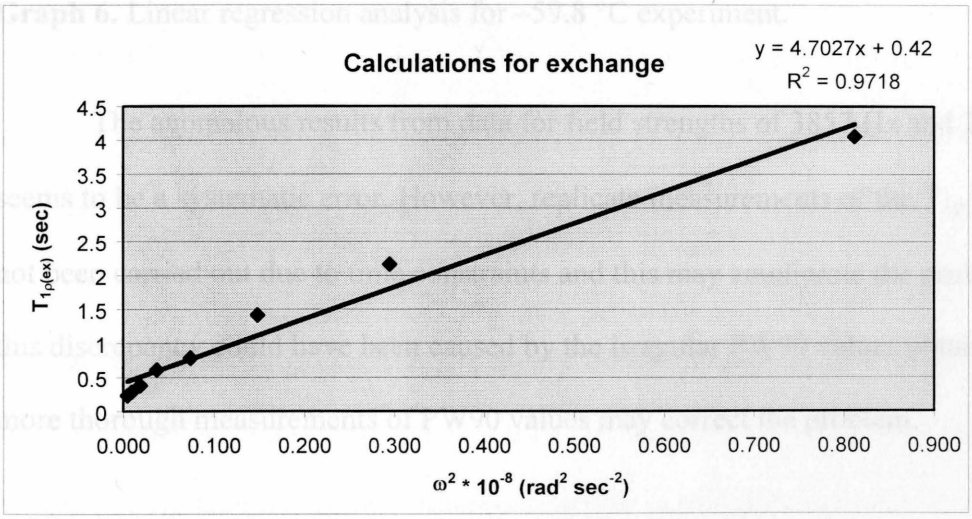

Graph 4. Linear regression analysis for –39.9 °C experiment.

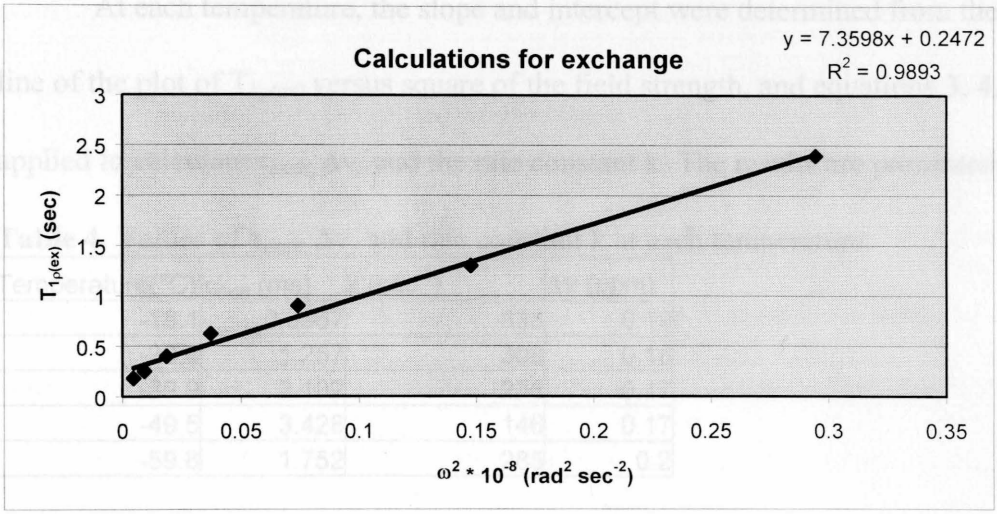

Graph 5. Linear regression analysis for –49.5 °C experiment.

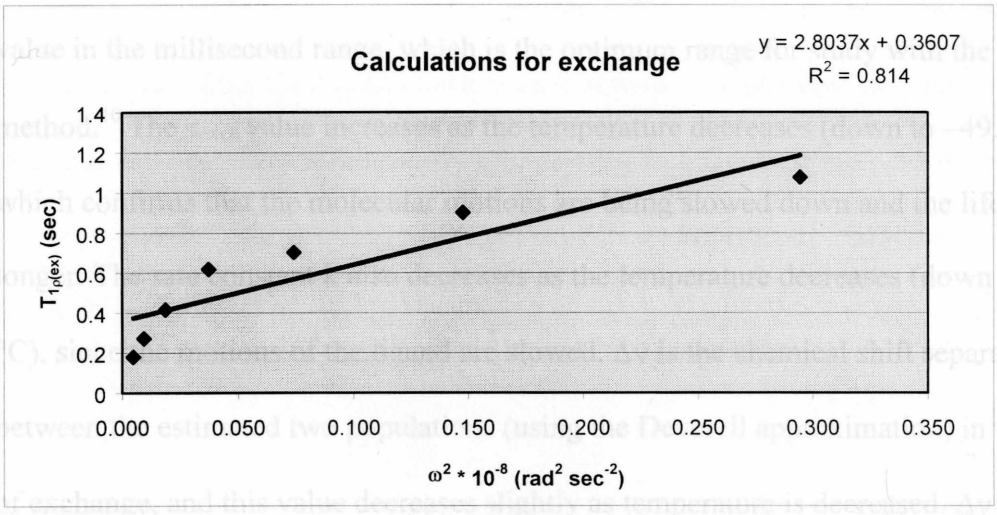

Graph 6. Linear regression analysis for –59.8 °C experiment.

The anomalous results from data for field strengths of 3857 Hz and 2731 Hz seems to be a systematic error. However, replicate measurements of the $T_{1\rho}$ values have not been carried out due to time constraints and this may ameliorate the problems. Also, this discrepancy could have been caused by the irregular PW90 values obtained, and more thorough measurements of PW90 values may correct the problem.

At each temperature, the slope and intercept were determined from the regression line of the plot of $T_{1\rho(ex)}$ versus square of the field strength, and equations 3, 4, and 5 were applied to calculate τ_{exch}, $\Delta\nu$, and the rate constant k. The results are presented in Table 4.

Table 4. Values of τ_{exch}, $\Delta\nu$, and rate constant k at each temperature.

Temperature(°C)	τ_{exch} (ms)	k (sec^{-1})	$\Delta\nu$ (ppm)
-19.1	0.5967	838	0.19
-29.4	1.257	398	0.18
-39.9	2.102	238	0.17
-49.5	3.428	146	0.17
-59.8	1.752	285	0.2

As the data show, at each of these temperatures the binaphthyl ligand **1** has a τ_{exch} value in the millisecond range, which is the optimum range for study with the $T_{1\rho}$ method.[10] The τ_{exch} value increases as the temperature decreases (down to –49.5 °C), which confirms that the molecular motions are being slowed down and the lifetime is longer. The rate constant k also decreases as the temperature decreases (down to –49.5 °C), since the motions of the ligand are slowed. $\Delta\nu$ is the chemical shift separation between the estimated two populations (using the Deverell approximation) in the absence of exchange, and this value decreases slightly as temperature is decreased. $\Delta\nu$ should not be affected by the decrease in temperature since $\Delta\nu$ is a value that occurs in the absence of exchange. That is, $\Delta\nu$ is the separation between the peaks when molecular motion is completely stopped and each conformer is frozen out. However, the differences between $\Delta\nu$ values are small, and they are likely identical within experimental error. Compared to the true separation estimated from the spectra obtained in the variable temperature NMR studies, which indicates a separation of 0.10 ppm between the peaks, the calculated separations are slightly greater. However, the true values and calculated values are in

good agreement with each other, particularly considering that the experimental value was estimated from peaks that were not fully resolved and that the 2-state approximation is not entirely accurate. It is important to note that upon fully freezing out the molecular motions, $\Delta\nu$ would be expected to be slightly greater than that observed to date.

The $\tau_{exch,}$ $\Delta\nu$, and rate constant k data at –59.8 °C do not conform to the trends observed, due to the poor regression equations obtained from the data points on Graph 6. This is most likely because the methoxy peaks on the spectra were not phased properly. As discussed above, it was not possible to phase the methoxy peak at each spin lock time τ individually with the Delta software, and this led to several of these peaks being much shorter or taller than they would have been if phased. The problem also occurred at other temperatures but it was more pronounced at –59.8 °C. This may have been caused by the fact that –59.8 °C is approximately the coalescence temperature. Thus, data from the –59.8 °C experiment was not included in the calculations of the activation parameters.

The activation barrier E_A is calculated using the Arrhenius equation

$$k = A \cdot e^{-E_A/RT} \tag{8}$$

where k is the rate constant, A is a frequency factor, E_A is the activation energy, R is the ideal gas constant, and T is the temperature in Kelvin.[11] By plotting ln k versus T^{-1} (Graph 7) and taking the slope to equal $-E_A/R$, the activation barrier between the conformations of ligand **1** can be obtained.

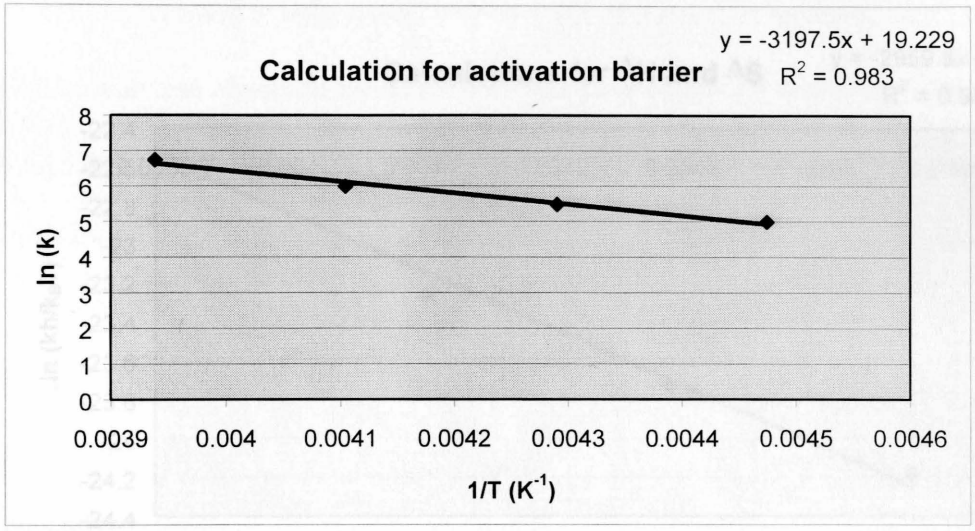

Graph 7. Regression analysis for derivation of E_A.

Thermodynamic parameters $\Delta H^{\ddagger}$ (enthalpy of activation) and $\Delta S^{\ddagger}$ (entropy of activation) were calculated using the Eyring equation:

$$k = \kappa \frac{k_B T}{h} e^{(-\Delta H^{\ddagger} + T\Delta S^{\ddagger})/RT} \qquad (9)$$

where k is the rate constant, κ is the transmission coefficient, k_B is Boltzmann's constant, T is the temperature in Kelvin, h is Planck's constant, and R is the ideal gas constant.[12] By plotting ln (kh/k_BT) versus T^{-1} (Graph 8), excluding –59.8 °C, and letting the slope equal $\Delta H^{\ddagger}/R$, and the intercept equal $\Delta S^{\ddagger}/R$, values for $\Delta S^{\ddagger}$ and $\Delta H^{\ddagger}$ can be calculated.

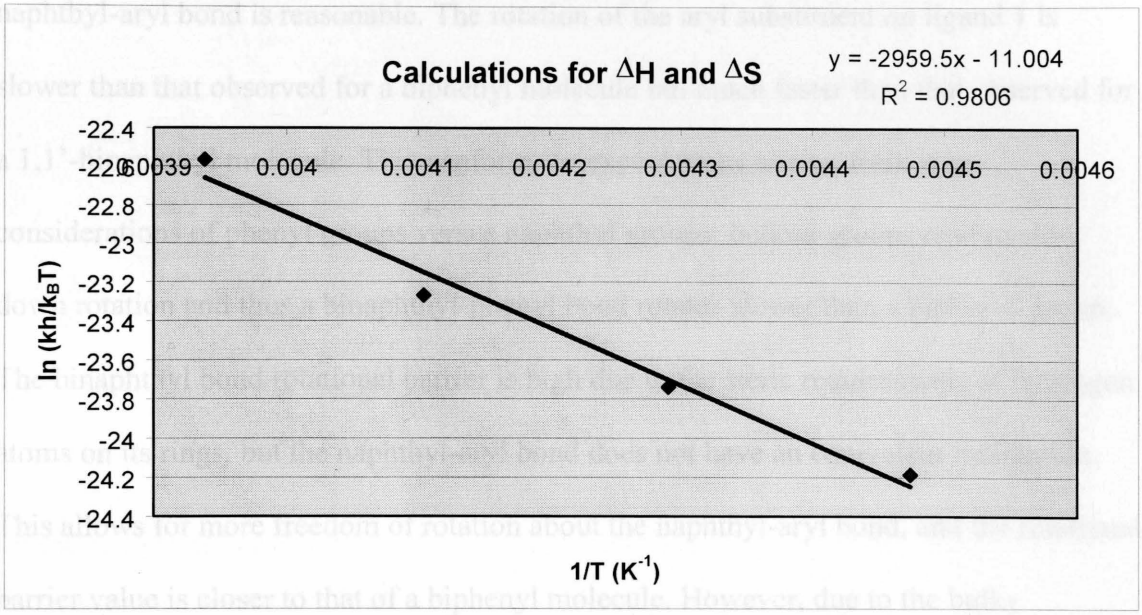

Graph 8. Regression analysis for derivation of $\Delta H^{\ddagger}$ and $\Delta S^{\ddagger}$.

$\Delta G^{\ddagger}$ values can be found with the thermodynamic equation:[11]

$$\Delta G^{\ddagger} = \Delta H^{\ddagger} - T\Delta S^{\ddagger} \qquad (10)$$

The activation energy and the thermodynamic parameters are presented in Table 6.

Table 6. Physical parameters of ligand **1**.

E_A (kcal/mol)	$\Delta H^{\ddagger}$ (kcal/mol)	$\Delta S^{\ddagger}$ (cal/mol)	$\Delta G^{\ddagger}$ (kcal/mol) (at 273 K)
6.4	6.0	-21	11.7

Comparing the activation barrier of the binaphthyl ligand (6.4 kcal/mol) to the activation barrier of the chair-chair flip of cyclohexane (10.1 kcal/mol)[13] and the activation barrier for butane rotation (3.2 – 6.1 kcal/mol),[13] it is clear that this value is relatively low. This points to a rapid exchange between the proposed conformations for ligand **1**. Computations done by Arulmozhiraja and coworkers show that a biphenyl has a rotational barrier of approximately 2.2 kcal/mol,[14] while another computation done by Kranz and coworkers shows that a 1,1'-binaphthyl molecule has a rotational barrier of 22.5 kcal/mol.[15] Compared to these values, the rotational barrier determined for the

naphthyl-aryl bond is reasonable. The rotation of the aryl substituent on ligand **1** is slower than that observed for a biphenyl molecule but much faster than that observed for a 1,1'-binaphthyl molecule. This conforms to expectations arising from size considerations of phenyl groups versus naphthyl groups; bulkier groups tend to slow down rotation and thus a binaphthyl-phenyl bond rotates slower than a biphenyl group. The binaphthyl bond rotational barrier is high due to the steric requirements of hydrogen atoms on its rings, but the naphthyl-aryl bond does not have an equivalent interaction. This allows for more freedom of rotation about the naphthyl-aryl bond, and the rotational barrier value is closer to that of a biphenyl molecule. However, due to the bulky substituents on the aromatic ring, the rotational barrier of ligand **1** is greater than that of a biphenyl molecule.

In polymeric ligand **3** (Figure 5), the aryl group is interacting with two naphthyl groups at the same time. The aryl group in ligand **4**, on the other hand, is interacting with one naphthyl group and one phenyl group, and thus it would be expected to have a lower rotational barrier. The rotational barrier values reported for binaphthyl and biphenyl molecules as well as the measured rotational barrier for ligand **1** support the conjecture that ligand **4** should be much more flexible, since its aryl group has greater freedom of rotation around its bonds. Also, such freedom of rotation increases the efficiency of coordination of ligand **4** to diethylzinc, since it allows each monomeric unit to be unhindered by the coordination activity of an adjacent monomeric unit and thus increases the population of the most favorable catalyst conformation.[4] These quantitative observations support the fact that upon modifying ligand **3** to ligand **4**, Pu observed a significant increase in reactivity coming from increased efficiency of coordination.[4]

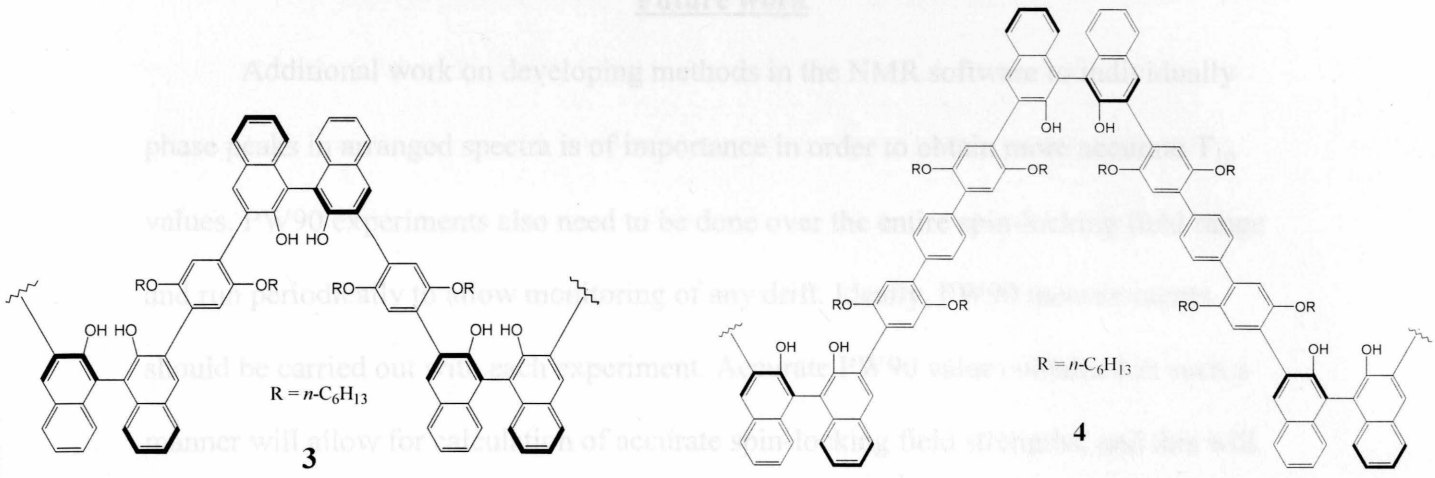

Figure 5. Polymeric ligands 3 and 4.

The studies on ligand **1** show that the $T_{1\rho}$ method is a powerful method for determining exchange rates of molecules, particularly those whose motions are too fast to be measured by the more traditional methods. Not only did the method show that ligand **1** has an exchange rate in the millisecond range (the optimum range for using the $T_{1\rho}$ methods) as predicted by its size, but the rate constants also allowed for calculation of the activation barrier and several thermodynamic parameters for the ligand. The relatively low rotational barrier points to a possible explanation of why a more rigid form of the polymeric ligand had a lower reactivity, and why the reactivity increased upon addition of a phenyl linker.

Future work

Additional work on developing methods in the NMR software to individually phase peaks in arranged spectra is of importance in order to obtain more accurate $T_{1\rho}$ values. PW90 experiments also need to be done over the entire spin-locking field range and run periodically to allow monitoring of any drift. Ideally, PW90 measurements should be carried out with each experiment. Accurate PW90 values obtained in such a manner will allow for calculation of accurate spin-locking field strengths, and this will lead to calculation of more reliable rate constants and activation parameters. The data inconsistencies from 3857 Hz and 2731 Hz for all temperatures and at 1536 Hz for –49.5 °C and –59.8 °C should also be eliminated by improved phasing and PW90 values. Inconsistencies will also be reduced by doing multiple runs at each temperature and taking more data points between dB values of 17 and 25. The data errors at –59.8 °C will also be checked with replicate measurements.

Other derivatives of the Pu system ligands with different substituents on the aryl substituents will be studied. Comparison studies similar to those carried out by Wang and Kopple on complex molecules[9] can be accomplished with different derivatives by first calculating $T_{1\rho}$ values using a two-population assumption. These will not be the true $T_{1\rho}$ values that will yield actual exchange parameters, but important comparisons can be made.

Variable temperature NMR studies suggest that ligand **1** has the same limiting conformations as ligand **2**, and it is already known that ligand **2** has three lowest energy conformations. Taking this information into account, the Deverell equations[8] for exchange rates and chemical shift should be expanded to accommodate a 3-state model,

which may be done by assuming the % distribution of the three isomers of ligand **1** to be equal to those of ligand **2**. This will yield more accurate results in exchange parameters amongst the 3 populations, and it will also present a more accurate description of the dynamics of ligand **1**.

Experimental Section

General. Air and moisture sensitive compounds were stored and manipulated in a nitrogen-filled Vaccum Atmospheres Nexus One glove box or under nitrogen on a Schlenk line.

Instrumentation. All simple ^{1}H NMR and dynamic NMR experiments were carried out on a JEOL Eclipse + NMR spectrometer operating at 400 MHz. The NMR temperature controller was calibrated with a methanol standard using established procedures.[6] Variable temperature experiments below –95 °C were carried out on a Varian Unity Inova 500/51 spectrometer at the Magnetic Resonance Lab of the University of Virginia.

Materials. Ligand **1** was prepared by David Moore of the University of Virginia.[16] CD_2Cl_2 packaged under nitrogen was purchased from Aldrich and used as received. $CDCl_3$ was purchased from Aldrich and used as received. Antimony pentachloride and antimony trifluoride packaged under argon were purchased from Aldrich and used as received. Dichlorofluoromethane-*d* (DCFM-*d*) was prepared according to literature procedure[5] and dried over molecular sieves prior to use.

DCFM-d.[5] Under nitrogen, 2 mL antimony pentachloride was placed into a septum vial, and the vial was capped. Antimony trifluoride (25 g, 0.14 mol, 1 equiv) was placed in an oven dried 250-mL 3-neck flask, and a large magnetic stir bar was added to the flask. Before weighing the solid, the bottle of antimony trifluoride was shaken to break up any chunks into a fine powder. The apparatus for the synthesis was assembled in the dry box

by fitting the 3-neck round bottom flask with a vacuum transfer arm, a glass stopper, and a septum. A 250 mL Schlenk flask with a Teflon valve was attached to a glass adaptor which was attached to the other end of the transfer arm, and all joints were secured with green Keck clips.

The septum vial and apparatus were removed from the dry box, and hoses were attached to the vacuum transfer arm and the Schlenk flask, which acts as the receiver flask. The hoses were put under N_2 via 4 pump/purge cycles, and the stopcocks to the transfer arm, the glass adaptor, and the Schlenk flask were opened to nitrogen. An ethyl acetate/liquid N_2 bath (–82 °C)[17] was prepared in a Dewar and placed around the receiver flask. While stirring, antimony pentachloride (1.5 mL, 0.0115 mol, 0.082 equiv) was added to the 3-neck flask via syringe, followed by chloroform-*d* (50 g, 0.42 mol, 3 equiv), also via syringe. The N_2 inlet was immediately closed to allow only simple venting to the bubbler so that the reaction could proceed under static N_2. The reaction began immediately, with bubbles appearing in the mineral oil bubbler within a few minutes. The rate of gas evolution was monitored so that only occasional bubbles appeared in the mineral oil bubbler. When too many bubbles appeared, the reaction mixture was cooled with an ice bath to slow the reaction. The reaction took about 45 minutes to complete, leaving a thick sludge in the 3-neck flask and the product (approximately 85 mL) as a clear colorless liquid in the receiver. The solvent was dried with molecular sieves that had been activated in the oven and cooled under vacuum. The solvent was stored under N_2 in the freezer and kept below its boiling point of 10 °C. The freezing point of dichlorofluoromethane-*d* is –135 °C, but it can be supercooled to –150 °C for an hour.[5]

Transfer of DCFM-*d* into a J-Young tube. A 250 mL Schlenk flask equipped with a Kontes valve adaptor and charged with DCFM-*d* was attached to a vacuum transfer arm. Since the solvent is a gas at room temperature, the Schlenk flask was kept cool in an ice bath. A male vacuum hose adaptor was attached at the other end of the vacuum transfer arm and the J-Young NMR tube (with sample to be analyzed already weighed into it) was attached via vacuum hose. The vacuum transfer line and the J-Young tube were placed under N_2 with 4 pump/purge cycles.

While under static vacuum, the J-Young tube was cooled in a small Dewar with an ethyl acetate/liquid N_2 cold bath (–82 °C).[17] The stopcock on the adaptor was opened slowly and the ice bath was lowered from the Schlenk flask. The Schlenk flask was gently warmed with the hand to coax the solvent into the J-Young tube. When the desired amount of solvent had been transferred, the stopcocks to the vacuum transfer arm and the Kontes valve adaptor were closed. Both the solvent flask and the NMR tube were stored in the freezer.

Procedures for NMR Experiments.

I. Pulsewidth 90 experiment

1) Log onto gfrance account.

2) Open up delta.

3) Click on button with NMR diagram on it, and type in wash_lee2 in server box in the window that comes up. Click on connect, and wait until connected to the instrument.

4) Click on 'sample' button on the NMR window. Load sample into NMR.

5) Check on the spin rate and solvent, and then click on the button with the picture of a lock. Wait for the NMR to lock.

6) Either choose 'Z1Z2' under 'Autoshim', or do a manual shim with the two knobs behind you.

7) Click on 'experiment' button on the bottom of NMR connection window.

8) Go to the global list by clicking on the picture of the globe, and then choose 'single_pulse.exp'. Rename file name and run the experiment.

9) When the 1D process comes up, it will already have processed the FID with the 'std_proton_autophase; list. Go to the list, click on 'ppm' and click on the delete button right above the list window. Then, go to 'process' and choose 'Hertz'. This will add a line that says 'Hertz' in the list window. Click on the 'process' button on the top right hand corner of the 1D processor window to let the spectrum show up in terms of kHz instead of ppm.

10) Choose the peak tool by clicking on the button to the top right hand corner of the spectrum and holding it down with the left mouse button while you choose the tool that looks like a diamond with a dot in the middle.

11) Click on the peak of interest with the peak tool. This will give you the peak value in kHz. Note the peak value as this is the x_offset value that you will be using.

12) Go to global list by clicking on the picture of the globe, and then click on 'service' on the left hand column, and double click on 'obs90_check.exp' on the right hand column to open up experiment.

13) Click on header button, and click on 'multifile' and then click the 'add' button. Make sure the 'multifile' choice is unclicked in the header before experiment.

14) Set the x_offset value with the kHz value of your peak of interest you found in step 8.

15) Change relaxation delay to 60 seconds (30 seconds is usually enough, but initially use 60 seconds. This value needs to be at least 5 time the T_1 value).

16) Array x_90_width from 1 to 51 μs at 5 μs steps (use linear array).

17) Start at 0 dB initially. Submit and run experiment.

18) Once experiment finishes, the nD processor comes up. Choose to view the first single slice by clicking on the '1D slice' button with the picture of a piece of bread. This brings up the 1D processor.

19) Press 'Ctrl+L' and then access global list by clicking on the button with a picture of a globe on it. Load the 'std_proton_autophase' list from the global list.. Then, press the button that says 'process' at the top right hand corner of window. This will process the FID and yield the spectrum.

20) Phase upon peak of interest using the ±90, ±5, and ±1 button to the right of the window with the spectrum of interest. The yellow tab (looks like a small upside down T) should be right under your peak of interest, and in the PP [%] window on the bottom right hand corner of the 1D processor window you should have the value of '50'. Press the Esc button.

21) This will transfer your process list into the nD processor. Draw data into the data slate by clicking on the button with a red arrow superimposed on several spectra. You can find this button towards the upper right hand corner of the nD processor window.

22) Once in the data slate, go to 'View' and make sure the 'Connect All' option is selected. Then, under the same 'View' menu, choose 'Vertical'.

23) After making sure the cursor turns yellow within the data slate by right clicking in the data slate (this selects the current window as the data to be processed), choose to expand array by going to Expand → Set dimension → Expand by Y.

24) Under the Expand menu again, choose 'Expand…'. Choose # slices to be 11, and arrow steps to be the value of the number of total slices – 11. The # slices at 11 seems to be the most optimum size as this allows us to view as many spectra without too much distortion.

25) Once the 11 data slices are displayed, zoom in on phased peak. Make sure that the window in which you're zooming in is the selected window. Check if arrow color is yellow in this window before you do this. If not, right click on the window of choice until the arrow turns yellow.

26) Find the first μs at which the peak seems to disappear altogether, which is the 180 degree point. Note that the peak of interest will decrease until it reaches a height of zero at 180° then becomes negative.

27) Re-run the experiment again, this time using values of ±5 μs from the apparent 180° area as the upper and lower bounds for the array. Use 1 μs steps. Add approximate 90° peak (found by dividing the crude 180 ° μs value by 2) in the beginning of array to allow easy phasing later on.

28) Find the μs at which the peak seems to disappear altogether. Then, re-run the experiment once more, using values of ±1 μs from the apparent 180° area as the upper and lower bounds for the array. Use 0.5 μs steps. Add approximate 90° peak in the beginning of array to allow easy phasing later on.

29) Find the μs at which the peak seems to disappear altogether for the 180° area. Usually 3 such iterations yield a good enough value at 180°, but refine as needed to get as precise a value as possible, always using the first scan as 90° to allow for easy phasing.

30) Repeat steps 26 to 29, for the μs value at 360°. The 360°pulse width is found by looking for the area in which the negative peaks (upside down peaks) seem to get smaller and pass through zero (360°) and then become positive.

31) Calculate the PW90 from the PW180 by dividing the μs value by 2, and calculate the PW90 from the PW360 by dividing the μs value by 4. Take the average of the two values for the PW90 value at 0 dB.

32) Repeat experiment steps 15 to 31 for each dB value needed. The PW90 will change with dB values, so the arrays need to be adjusted accordingly. PW90 is approximately 8.9 μs at 0 dB, and doubles for each 6 dB increase in the attenuator strength. So the approximate PW90 values can be calculated in advance and the arrays for the experiments adjusted accordingly. After finding the proper PW90 values, the formula field strength = 1/(4*PW90), where PW90 is in seconds, can be used to calculate the field strength.

II. NMR setup for VT experiments[18]

1) Note freezing point of solvent. Do not go lower than 10° above the freezing point, with the exception of DCFM-*d*, which can be supercooled to -150°C for short periods of time.[5]

2) Fill Dewar with liquid N_2 using a funnel, and the steps as a prop for the metal dispenser hose. Stop once liquid N_2 starts boiling up around the interface between the funnel and the Dewar. Do not overfill Dewar.

3) Once Dewar is filled, place heating element into the Dewar. Be careful not to place the heating element in too quickly as this will cause too much liquid N_2 to boil off from the Dewar. Screw the heating element on securely once in place.

4) Detach the air hose from the bottom of the NMR (this hose is clear with a gray attachment end), and attach the elephant nose of the Dewar in its place.

5) Attach the Dewar heating element power supply to Dewar. This wire is labeled 'Dewar heater' and has a square attachment end.

6) Log onto gfrance account.

7) Log onto delta.

8) Log onto the NMR by typing in wash_lee2 in the node box and clicking on the connect button.

9) Once connected, open up the sample window.

10) Eject standard.

11) Once standard is ejected, close the valve labeled 'air'. At this point, you should hear a stop in the sound of air flow.

12) Open up the valve labeled 'N2' all the way.

13) Open up the main valve on the liquid N_2 tank.

14) Open up the small valve on the liquid N_2 tank. At this point, you should hear the air flow resume. Make sure the regulator pressure is at 20 (look at the circular gauge on the left for this).

15) Place sample into the NMR, and load.

16) Check sample is spinning at around 15 Hz, and allow 5 mins for the NMR to purge.

17) Set NMR to desired temperature. Cool or warm up in increments of 10 degrees. Allow 5 to 10 minutes of equilibration at target temperature.

18) Set up and run experiment.

19) Keep track of time NMR is run with N_2. One tank will allow **~26 hours** of experiments.

Note: With DCFM-*d* as solvent, you must cool the NMR to below 10°C before inserting sample. You should note that failing to do this could blow up the J-Young tube in the NMR probe!!!

III. T_1 experiment

1) Setup the NMR for VT experimentation. (See experiment II)

2) Drop temperature to desired temperature in increments of 10 degrees.

3) Wait 5 to 10 minutes for the sample to equilibrate.

4) Click on the 'Sample' button on the NMR window.

5) Check on sample spin rate and solvent, and then click on the button with the picture of a lock to have the NMR lock onto the sample.

6) Either choose 'Z1Z2' under 'Autoshim' or manually shim with knobs behind you.

7) Click on the 'Experiment' button on the NMR window.

8) Click on the globe to access the global list of experiments. Double click on the single_pulse.exp on the right hand column.

9) Rename file name and sample ID, and run a simple ^{1}H-NMR.

10) Once data is collected, 1D processor should appear automatically with your FID already processed. If you are opening up a previously collected spectrum, make sure to

load list 'std_proton_autophase' list and process the data. **Make sure the spectrum is in MHz instead of ppm**. To do this, go to the list window, click on 'ppm' and click on the delete button right above the list window. Then, go to 'Display' and choose 'Hertz'. This will add a line that says 'Hertz' in the list window. Click on the 'process' button on the top right hand corner of the 1D processor window to let the spectrum show up in terms of kHz instead of ppm. This yields a more precise value for x_offset.

11) Zoom in on peak of interest, and choose the peak tool by clicking on the upper right hand corner of the spectra and choosing the tool that makes the cursor into a diamond with a dot in the middle. With the peak tool, find out the Hz value of the peak by clicking on the peak of interest. This will be your x_offset value for the rest of the T_1 and $T_{1\rho}$ experiments at this temperature. The x_offset value needs to be checked every time before you run your set of $T_1/T_{1\rho}$ experiments.

12) Click on the 'Experiment' button on the NMR window again. Click on the globe to access the global list, and then click on 1d_more on the left column, then double click on the double_pulse.exp on the right column.

13) Rename filename, and make sure that the sample ID is the same as that of the H-NMR sample ID (at step 4).

14) Use the following parameters for the experiment:

process: nD processor

x_offset : [kHz] value of the peak of interest found with simple H NMR spectrum at step 11.

x_sweep : 9 [ppm] (This value may change for other BINAP molecules studied; I

am currently studying the *t*-butyl BINAP molecule. This value is chosen to yield the full spectrum with the peak of interest in the center.)

scan: 4

prescan: 0

relaxation delay: 60 seconds

τ interval: exponential array, from 0.1 seconds to 50 seconds, 10 points (This array may be changed with other molecules)

The total time for the experiment is around 50 minutes. However, this value can change when x_sweep, # scans/prescans, relaxation delay, and τ interval values are altered.

15) Submit experiment. Workup according to procedures on experiment VII : How to workup data for T_1 and $T_{1\rho}$ experiments. Note that a T_1 experiment must be run first with every set of $T_{1\rho}$ experiments, as the T_1 value is needed to calculate the $T_{1\rho(ex)}$ value.

IV. $T_{1\rho}$ experiments

$T_{1\rho}$ experiments were carried out in sets of 10 at temperatures ranging from –20 to –60 (in 10 degree increments) on the coalesced peak of interest. dB values of 17, 20, 25, 30, 33, 36, 39, 42, 45, and 48, were used for the $T_{1\rho}$ experiments, and a T_1 experiment was also run at the beginning of each batch of $T_{1\rho}$ experiments as the T_1 value was needed later for calculations. Each $T_{1\rho}$ experiment took around 22 minutes, and the T_1 experiment took around 50 minutes. Thus, each set of experiments took between 4 to 5 hours.

The $T_{1\rho}$ experiments involve spin-locking the bulk magnetization vector in the xy plane with spin-locking field $\mathbf{B_2}$. The strength of $\mathbf{B_2}$ is adjusted by changing the dB values. The bulk magnetization vector is first hit with a 90° pulse to send it into the xy plane, and then it is locked with $\mathbf{B_2}$ for an array of spin-locking time τ. The rate of decrease in the bulk magnetization vector yields the $T_{1\rho}$ values. The pulse sequence for measuring T1 was $90°_x$-$(\text{spin-lock})_y$-acquire.

1) Set up the NMR for VT experimentation. (See experiment II)

2) Drop temperature to desired temperature in increments of 10 degrees.

3) Wait 5 to 10 minutes for the sample to equilibrate.

4) Click on the 'Sample' button on the NMR window.

5) Check on sample spin rate and solvent, and then click on the button with the picture of a lock to have the NMR lock onto the sample.

6) Either choose 'Z1Z2' under 'Autoshim' or manually shim with knobs behind you.

7) Click on the 'Experiment' button on the NMR window.

8) Click on the button with the picture of the house on it to access the home directory. Double click on 'spinlock.exp' to open up window for the $T_{1\rho}$ experiments.

9) Rename file name and sample ID. Match the sample ID you used for your simple ^{1}H-NMR and T_1 experiments on experiment III. This will allow you to queue up experiments and have them run one after the other without having to hit 'go' between each experiment.

10) Use the following parameters:

processor : nD processor.

x_offset : kHz value of peak of interest from simple ^{1}H NMR

x_sweep: 9[ppm] (for current *t*-butyl BINAP compound)

scans:4

prescans:1

spinlock_atn: change from 17 to 48 for each file. (dB values I used : 17,20,25,30,33,36,39,42,45,48) **Do not run it below 15 dB!**

relaxation delay: 7s

spinlock time: This value needs to be tailored for each dB at each temperature. Initially start out with an exponential array from 0.01 seconds to 4 seconds, with 21 points. This will allow you to see the appropriate range of points you should start collecting on the next repeat of the experiment. Each dB/temperature combination should be carried out 3 times to ensure regularity, and try to use around 20 points. If using 20 points does not allow the last point to have a spin lock time at the value that you've chosen, change # points around a bit to make the last point have the upper bound value as its spin lock time value. **Note number of points used per spectrum; this makes dealing with the data slate much easier later!**

11) When data is collected, an nD processor window pops up automatically. Use the experimental VII for details on workup.

V. Data workup for T_1 and $T_{1\rho}$

1) Once data finishes collecting, an nD processor window pops up automatically.

2) For T_1 experiments, open up the 1D slice with the longest τ value. You can get to the last spectrum by scrolling through the right arrow bar next to the 'Y' button, while having the 'X' button depressed. Then, click on the button '1D slice'.

3) For $T_{1\rho}$ experiments, simply click on '1D slice' button once the nD processor comes up. This allows you to process the first slice.

4) Upon opening the 1D slice in the 1D processor, hit Ctrl+L to open up a process list. At the global list, choose 'std_proton_autophase.list' and click on 'ok'.

5) Click on 'process' button on the upper right hand corner of the 1D spectrum window.

6) Once FID is processed, zoom in on peak of interest. If things were done according to procedures above, this peak should be set at 50% (i.e. middle of the spectrum).

7) Using the ±90, ±5, and ±1 buttons on the right of the spectrum, you should manually phase this peak as well as possible.

8) Hit the escape button.

9) You should see the process list appear under the window with the 'X' button depressed. Now, click on the button with a red arrow overlapping some spectra towards the upper right hand corner of the nD processor window. This should transport the data onto the data slate. Maximize data slate at this point.

10) Under 'View', make sure the 'Connect All' option is selected. Then, choose 'Vertical'.

11) After making sure the cursor turns yellow within the data slate (i.e. selected window is the data to be processed) by right clicking in the data slate window, go to Expand → Set dimension → Expand by Y.

12) Under the Expand menu again, go to 'Expand…'. Make sure you're selecting the option with the three periods after the word 'expand'.

13) Choose 11 slices for number of slices (this seems to be the optimum size for most experiments for me as it displays the most spectra with the least distortion; can be less if you want to). Arrow step will adjust to 11 also, but change it to the number that you obtain after subtracting 11 from the number of total points used for generation of spectrum. (See experiment IV, step 10). Click on OK.

14) This should generate a page with 11 spectra plus your original data containing all dimensions. Press Alt + F to get rid of the file name and only get the spinlock time values on each spectra.

15) After making sure your cursor is yellow in the **second window** (which is NOT the original data window but the one to the right of it) by right clicking in it, zoom into the peak of interest. All other windows should zoom into the same peak in the same manner. This allows for comparison between peaks as this scales the peak in the same manner in all windows.

16) Now, to view the rest of the peaks, make sure the cursor is yellow in the **original data window** (the first window of the data slate) by right clicking in it. Then, click on the arrow button (pointing right) on the upper right hand corner of the window. This should scroll to the rest of the spectra of your experiment. **Note that if the arrow step does not match the exact number of spectra left after your first 11, the data slate will not step through to them!** If you need to change the arrow step, go to 'Expand' and to 'arrow step' and adjust arrow step as needed. **Also, note that if your cursor is yellow in the second window and you try to step through the slices, the program will attempt to**

step through the slices of the second spectra only, and will get very confused. Stepping through slices should not take more than 4 to 5 seconds. Note also that overlap of certain spectra can occur between the two pages that you're viewing.

17) Print the 1 to 2 pages of slices for record (for T_1) or manual calculations ($T_{1\rho}$) later.

18) Now in the delta window (the initial window where you selected to log onto the NMR), go to 'Viewers' and choose 'T_1 analyze'.

19) To analyze the $T_1/T_{1\rho}$ values, first click on the button with the picture of the hand with an extended finger. Then, click on the button right next to it, with the picture of a folder with a curved arrow on it. Click on the orginial data window to bring the data into the T_1 analyze viewer.

20) For the T_1 value, scroll with the right arrow button all the way to the last spectra (always try to use the spectra with your peak at its maximum size). After making sure the button 'By Pick' is depressed, scroll into the peak of interest. Then, with the cursor, try to pick the center of the peak as best as you can (this is easier when you zoom into the peak a lot so that your peak is broadened). After clicking on the 'apply' button, choose 'Weighted Linear Inversion Recovery' on the left hand column window. This should yield T_1 and σ values. Note values in notebook. Also choose 'Unweighted Linear Inversion Recovery' and note T_1 and σ values.

21) For the $T_{1\rho}$ value, use the first spectrum that appears. After making sure the button 'By Pick' is depressed, zoom into the peak of interest. Then, with the cursor, try to pick the center of the peak as best as you can (this is easier when you zoom into the peak a lot so that your peak is broadened). After clicking on the 'apply' button, choose 'Weighted Linear Spinlock' on the left hand column window. This should yield T_2 (which in reality

are $T_{1\rho}$ values) and σ values. Note values in notebook. Also choose 'Unweighted Linear Spinlock' and note T_2 and σ values.

VI. Temperature calibration experiments[6]

1) Take a clean NMR tube and a cap into the dry box via the small antechamber.

2) Once in the box, charge NMR tube with 0.5 to 0.75 mL CD_2Cl_2.

3) Insert the sealed tube of neat MeOH into the NMR tube and parafilm at the seal. The CD_2Cl_2 provides a deuterium signal on which the NMR can lock.

4) Setup NMR for VT experiment according to procedures of experiment II.

5) Drop temperature down to –90 degrees in 10 degree increments. Allow 5 to 10 minutes for the sample to equilibrate.

6) Take a simple ^{1}H-NMR at this temperature. Make sure the autogain feature is selected for sharp, well-phased peaks.

7) Once the 1-D spectrum is obtained, use the peak picking tool (looks like a diamond with a dot in the middle) to select the first peak and get its δ value.

8) Use the same tool to click on the second peak and get its δ value.

9) While holding down the Alt key, click on the first peak to select it; δ value turns yellow, and a '#' symbol appears above this peak.

10) Choose the 7th tool in the peak tool menu bar (it's the button with an arrow with a small diamond with a dot in the middle). While holding down the Alt key, click on the second peak to select it. The δ value turns yellow, and '#' symbol appears above this peak.

11) Press J to obtain separation in Hz.

12) Repeat steps 5 through 11, changing the temperature by 5 degree increments at first up to 70 degrees. Then, change the temperature by 10 degree increments up to 20 degrees. Always allow 10 minutes at each temperature for equilibration.

13) With the recorded J values, calculate the actual temperature of the NMR, using the temperature calculator on www.spectroscopynow.com/Spy/tools/temperature.html. The equation used to calculated the temperature is T (Kelvins) = 409.0 - 36.54·Δδ - 21.85·$(\Delta\delta)^2$.[19] Use 399.7841973 MHz as the proton hertz value.

14) Plot Actual Temperature vs. Set Temperature.

15) Using linear regression, determine the equation for calculating the actual temperature from the set temperature. The equation obtained from the experiment was: Actual temperature = 1.0213(set temperature) + 1.4207. Experiment showed that the real temperature that the NMR probe reached was close to the set temperature on the computer. The lower temperatures were shown to have higher correlation between the set temperature and the real temperature. Temperature calibration experiments should be repeated periodically.

Table 7. Temperature calibration data.

Set Temperature (C)	Actual Temperature (C)
20	21.6
10	12.3
0	1.4
-10	-8.8
-20	-19.1
-30	-29.4
-40	-39.9
-50	-49.5
-60	-59.8
-70	-70.0
-75	-75.2
-80	-80.3
-85	-85.2

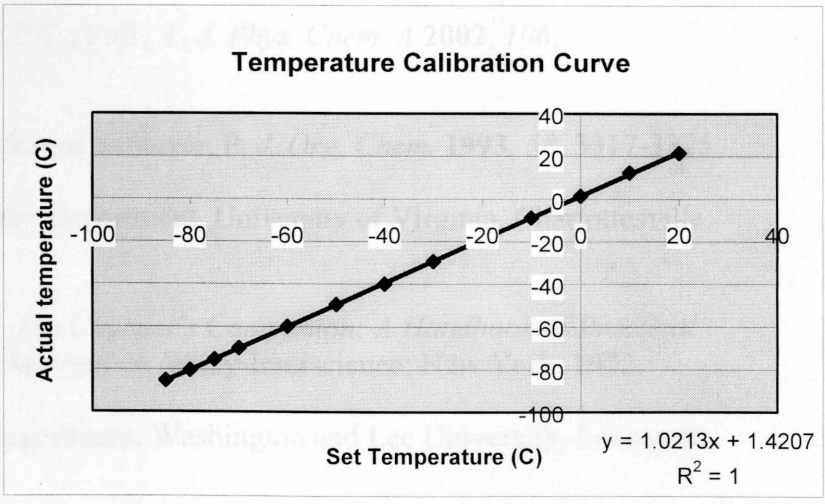

Graph 9. Linear regression analysis on data of Table 7.

References

(1) Noyori, R.; Kitamura, M. *Angew. Chem. Int. Ed. Engl.* **1991**, *30*, 49-69.

(2) Soai, K.; Niwa S. *Chem. Rev.* **1992**, *92*, 833-856.

(3) Huang, W.-S.; Hu, Q.-S.; Pu, L. *J. Org. Chem.* **1998**, *63*, 1364-1365.

(4) Simonson, D.; Kingsbury, K.; Xu, M.-H.; Hu, Q.-S.; Sabat, M.; Pu, L. Submitted to *Tetrahedron.*

(5) Siegel, J. S.; Anet, F. A. L. *J. Org. Chem.* **1988**, *53*, 2629-2630.

(6) Braun, S.; Kalinowski, H.-O.; Berger, S. *150 and More Basic NMR Experiments – A practical course*. Wiley-VCH: New York, 1998; pp.136-139.

(7) Wang, Y.-S. *Concepts Magn. Reson.* **1992**, *4*, 327-337.

(8) Deverell, C.; Morgan, R. E.; Strange, J. H. *Mol. Phys.* **1970**, *18*, 553-559.

(9) Kopple, K. D.; Wang, Y.-S., Cheng, A. G.; Bhandary, K. K. *J. Am. Chem. Soc.* **1988**, *110*, 4168-4176.

(10) Wang, Y.-S.; Ikuta, S. *Magn. Reson. Chem.* **1989**, *27*, 1134-1141.

(11) Sandström, J. *Dynamic NMR Spectroscopy*; Academic Press: New York, 1982.

(12) Eyring, H. *Chem. Rev.* **1935**, *17*, 65.

(13) Loudon, G. M. *Organic Chemistry*, 3rd ed.; The Benjamin/Cummings Publishing Company, Inc.: Redwood City, CA, 1995.

(14) Arulmozhiraja, S.; Selvin, P.C.; Fujii, T. *J. Phys. Chem. A* **2002**, *106*, 1765-1769.

(15) Kranz, M.; Clark, T.; von Ragué Schleyer, P. *J. Org. Chem.* **1993**, *58*, 3317-3325.

(16) Moore, D.; Pu, L. Chemistry Department, University of Virginia, Charlottesville, VA.

(17) Gordon, A. J.; Ford, R. A. *The Chemist's Companion: A Handbook of Practical Data, Techniques, and References*; Wiley-Interscience: New York, 1972.

(18) Trimmer, P., Chemistry Department, Washington and Lee University, Lexington, VA.

(19) Amman, C.; Meier, P.; Merbach, A. E. *J. Magn. Reson.* **1982**, *46*, 319-321.